LONG-TERM CRANIAL RECONSTRUCTIONS IN FULL THICKNESS DEFECTS USING CARBONATED CALCIUM PHOSPHATE CEMENT WITH TITANIUM MESH SCAFFOLD IN A SHEEP MODEL: BIOMECHANICAL ANALYSIS

A Thesis

Presented to

The Graduate Faculty of The University of Akron

In Partial Fulfillment

of the Requirements for the Degree

Master of Science

Anand Parikh

December, 2006

LONG-TERM CRANIAL RECONSTRUCTIONS IN FULL THICKNESS DEFECTS USING CARBONATED CALCIUM PHOSPHATE CEMENT WITH TITANIUM MESH SCAFFOLD IN A SHEEP MODEL: BIOMECHANICAL ANALYSIS

Anand Parikh

Thesis

Approved:

_____
Co-Advisor
Dr. Glen O. Njus

_____
Co-Advisor
Dr. Daniel B. Sheffer

_____
Faculty Reader
Dr. Mary C. Verstraete

Accepted:

_____
Department Chair
Dr. Daniel B. Sheffer

_____
Dean of the College
Dr. George K. Haritos

_____
Dean of the Graduate School
Dr. George R. Newkome

_____
Date

ABSTRACT

Autogenous bone graft (ABG) is considered the evaluation standard for cranial defect reconstruction material. A variety of bone substitutes have been used as alternative materials for this procedure, each having its own advantages and disadvantages. Carbonated calcium phosphate (CCPP), a biomaterial form of hydroxyapatite (HA), has been increasingly used for cranial reconstructions. For defects of certain size and shape, CCPP is used with a titanium mesh for structural stability.

At the present time there have been no published studies in the literature comparing the biomechanical and histological properties of these cranial bone reconstruction structures over time. In this study two different reconstruction structures were compared to autogenous bone grafts with respect to time. Reconstruction structure A (RCA) used a slow setting CCPP, whereas reconstruction structure B (RCB) used a fast setting CCPP.

Unilateral or bilateral cranial defect reconstructions were conducted on sheep with full thickness defect sizes of 1.5 × 3.0 cm. A total of 24 sheep were divided into eight groups with post surgical periods of 0, 6 and 12 months. The skulls' biomechanical properties were evaluated using a free weight drop test protocol. In addition, intact parietal bone was also evaluated at 12 months as a control.

Peak acceleration, peak force transmission and time to peak acceleration parameters obtained from the drop weight test were used for analysis.

Immediately post-surgery there were no significant differences in any biomechanical characteristics of the experimental groups. At 12 months, the autogenous bone graft (ABG) reconstructions had a significantly superior impact characteristic compared to reconstructions of slow setting CCPP with titanium mesh scaffold and reconstructions of fast setting CCPP with titanium mesh scaffold ($p<0.05$). At 12 months ABG was not significantly different from the intact bone ($p>0.05$).

ACKNOWLEDGMENTS

I would like to express my deepest and sincere gratitude to my research advisor Dr. Glen Njus for his constant guidance, encouragement and unwavering support towards this project. I owe special thanks to Dr. A. Seth Greenwald, Mr. Paul Postak, and Ms. Christine Heim, of Orthopaedic Research Laboratories for providing invaluable experience and training to handle projects during my Summer Internship. My sincere thanks to Dr. Andrea Gonzalez who assisted me with the experimental testing and literature review. I am thankful to Dr. James Zins, Orthopaedic Research Laboratories and Synthes Maxillofacial, CO, USA for granting me permission to incorporate the study into my Masters Thesis.

I would like to extend my thanks to my committee members Dr. Daniel Sheffer and Dr. Mary Verstraete for their invaluable insights and suggestions. I would like to thank Mr. Dick Reed for his help on test jig development. Lastly, thanks to all my friends and parents for their love and affection.

TABLE OF CONTENTS

Page

LIST OF TABLES

LIST OF FIGURES

CHAPTER I

INTRODUCTION

1.1 Overview

A part of this project was assigned during my internship with Orthopaedic Research Laboratories, Lutheran Hospital, Cleveland Clinic Health System, Cleveland, OH during Summer 2005. One of my choices was the complete evaluation of sheep skulls, from a study where defects were reconstructed using carbonated calcium phosphate (CCPP) cement with a titanium mesh scaffold. This included apparatus selection, biomechanical test protocol, test jig design, calibration, testing and data analysis.

The sheep skull samples with pertinent information on how the sheep skulls were reconstructed were provided by the Department of Plastic Surgery, The Cleveland Clinic Foundation, Cleveland, OH. The experimental testing was carried out at Calhoun Research Lab, Akron General Medical Center, Akron, OH; under the guidance of Dr. Glen Njus, Research Associate Professor, Department of Biomedical Engineering, The University of Akron, Akron, OH. The experimental tests were assisted by Dr. Andrea Moreira-Gonzalez, a research fellow under the principal investigator for the project, Dr. James Zins, Chairman, Department of Plastic Surgery, The Cleveland Clinic Foundation, Cleveland, OH. A report concerning experimental analysis has been submitted to Dr.

James Zins and Christine Heim, Operations Manager, Orthopaedic Research Laboratories, who was my supervisor for the project during my internship.

1.2 Cranial Defect Reconstruction

Defects in the cranial skeleton which require reconstruction include tumor resection, congenital deformities, craniotomies for neurosurgical approaches, and trauma [39]. The autogenous bone graft is considered the gold standard for cranial reconstruction. To augment its use, a variety of bone substitute materials have been evaluated, each having its own advantages and disadvantages. An extensively used biomaterial for cranial reconstruction has been hydroxyapatite (HA). Carbonated calcium phosphate (CCPP) is a form of HA, which is claimed to offer significant advantages over the existing biomaterials used [1,2,3,5,6,7,8,12,13,14,15,17,21,25,31,40].

With respect to time, however, the use of CCPP is unknown. A clinical uncertainty associated with the use of CCPP is its immediate biomechanical properties, and over time as the reconstruction becomes incorporated. In this study cranial reconstructions were conducted on sheep models with what has been termed critical sized defects of 1.5 × 3.0 cm [28]. This defect was four sided with the enclosed four angles equal to 90±6 degrees. Reconstruction techniques were either slow setting reconstruction structure (RCA), fast setting reconstruction structure (RCB), or autogenous bone grafts (ABG). All surgeries were either unilateral or bilateral reconstructions of cranial defects in sheep skulls. For the RCA reconstruction, relatively slow setting (10 minutes) CCPP cement was used with an underlying titanium mesh between the cement and dura. RCB reconstruction was similar with the exception that a relatively fast setting (less than 5minutes) CCPP cement was used.

No data are available in the literature comparing the biomechanical and histological properties of RCA and RCB in cranial bone reconstruction over time. This study examines the biomechanical properties of RCA, RCB, and ABG over time. The sheep were sacrificed at time t_0 (immediate sacrifice), t_1 (6 months), and t_2 (12 months). The sheep skulls were experimentally tested using drop weight testing. Statistical analyses were performed to compare RCA, RCB, and ABG on different biomechanical parameters obtained by drop weight testing. Comparisons were conducted to find whether any interaction effect existed between the reconstructions over a period of time. Intact bone (control group), with no reconstructions were tested after a 12 month period. Statistical analyses were also performed to compare the biostructural characteristics of RCA, RCB, and ABG with respect to intact bone at t_2 (12 month).

1.3 Significance of the Study

The clinical significance of this study was to compare the biomechanical properties of the two reconstruction structures (slow setting and fast setting carbonated calcium phosphate cements with titanium mesh scaffold) and autogenous bone grafts on critically sized full-thickness reconstructions of cranial bone defects. The global study was documented for the reconstruction efficacy, biomechanical characteristics, and histological findings over time. As previously stated, the time periods were t_0 (immediate sacrifice), t_1 (6 months), and t_2 (12 months) post-surgery in the sheep model. Findings assisted in determining whether there is a need for improvement over the existing synthetic technique, which can be used as an alternative for cranial defects reconstruction.

1.4 Hypothesis Testing / Objective of Study

This study compared the biomechanical properties of the reconstruction structures RCA, RCB, and ABG by using impact testing (rapid loading technique) for experimental analysis of the cranial bone defects in a sheep model. The sheep skulls were tested based on their postoperative period at time t_0 (immediate sacrifice), t_1 (6 months), and t_2 (12 months) after reconstruction.

1.4.1 Null Hypotheses

1. There is no significant difference in the biomechanical properties of the reconstruction structures RCA, RCB, and autogenous bone graft (ABG) with respect to time periods of t_0 (0 month), t_1 (6 months), and t_2 (12 months).

2. There is no significant difference in the biostructural characteristics between RCA, RCB, and ABG with respect to the intact bone at t_2 (12 months) period.

1.4.2 Alternate Hypotheses

1. There is a significant difference in the biomechanical properties of the reconstruction structures RCA, RCB, and ABG with respect to time periods of t_0 (0 month), t_1 (6 months), and t_2 (12 months).

2. There is a significant difference in the biostructural characteristics between RCA, RCB, and ABG with respect to the intact bone at t_2 (12 months) period.

CHAPTER II

LITERATURE REVIEW

2.1 Anatomy of the Human and Sheep Skull

Typically, there are 206 bones in the body, though there may be up to approximately 226. Of these there are 22 bones of the skull, which include 8 cranial and 14 facial bones [45].

Table 1. List of the 22 bones of Human Skull

8 Cranial Bones	1 x Ethmoid Bone
	1 x Frontal Bone
	1 x Occipital Bone
	2 x Parietal Bones
	1 x Sphenoid Bone
	2 x Temporal Bones

14 Facial Bones	2 x Inferior Nasal Conchae
	2 x Lacrimal Bones
	1 x Mandible
	2 x Maxillae
	2 x Nasal Bones
	2 x Palatine Bones
	1 x Vomer
	2 x Zygomatic Bones

The cranium is the part of the skull that holds and protects the brain in a cavity, called the cranial vault. Eight cranium bones join together at joints called sutures [44,45].

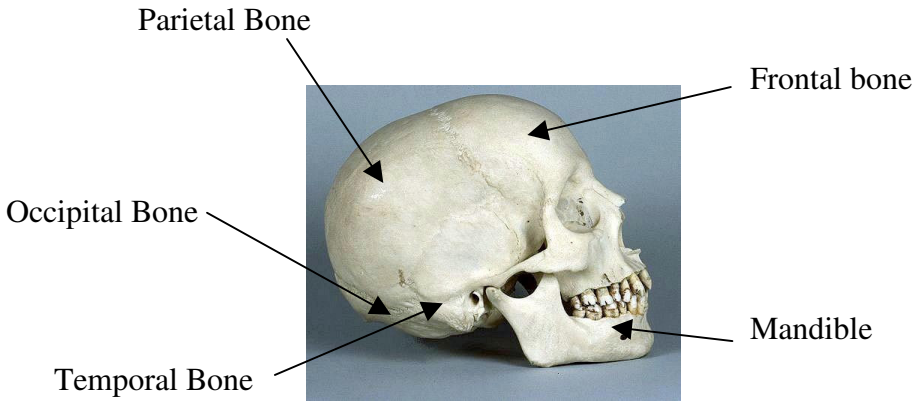

Figure 2.1. Human Skull [49].

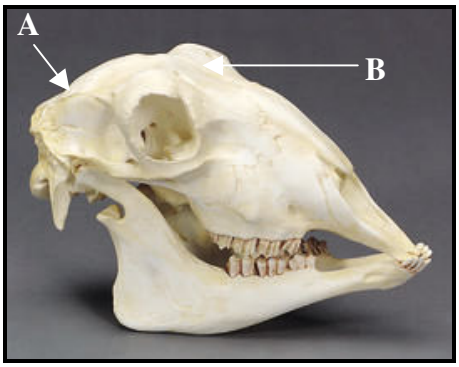

Figure 2.2. Sheep skull [47]. Parietal bone (A), and frontal bone (B) are shown.

One function of the cranium is the protection of the neural matter. Cranial bones inner surfaces attach to membranes that stabilize the positions of the brain, blood vessels, and nerves. Outer surfaces of the cranial bone act as areas of attachment for muscles that move the head in various ways [45].

Personal conversation with Dr. Andrea Moreira-Gonzalez provided information that sheep are similar to man in bone structure and mineral metabolism. In a skeletally mature sheep, the calvarial parietal bone thickness resembles that of a human cranium, 2-3mm. Sheep skulls are of sufficient size that it is possible to create bilateral full-thickness skull defect [28].

2.2 Cranial Bone Defect Reconstructions

Cranial bone defects treated with autogenous bone grafts have been considered as the gold standard for reconstruction. Cranial bone, iliac bone, and ribs are used as bone graft donor sites. Cranial bone is advantageous over iliac bone or ribs due to its proximity to the surgical site, harvesting ease, and structure. In addition, the consistency of cortical bone mineral density and having a rich haversian network allow vascularization to occur more rapidly. Limitations cited for the use of autogenous bone graft include donor site morbidity and increase in operation times. Moreover, cranial bone also undergoes unpredicted amount of resorption, leading occasionally to a secondary reconstruction and is unreliable for long term augmentation [2,3,14,15,27,30,33,40].

Gold and silver were initially used as alloplastic implantable substitutes for bone grafts. Due to their inability to withstand even minor trauma and difficulty in shaping, they were discarded. This led to the use of metals and alloys, such as stainless steel, vitallium, and tantalum. Vitallium is a rigid material that cannot be tailored in the

operating room. Stainless steel had found use over tantalum due to its low cost. The main advantage of these alloys is that they are less corrosive than other metals. But these metals are intolerant of changes in weather due to heat and cold conduction, skin breakdown, and extrusions, thus leading to the end of their widespread use [2,7,9,32,42].

An ideal bone replacement substitute for cranial defect reconstruction would need to be biocompatible with surrounding tissue, radiolucent, easily shaped or molded, able to achieve cosmetic restoration, non-allergic and non-carcinogenic, able to achieve similar resistance to deformation, strong enough to endure trauma, stable over time, able to maintain volume, and osteoactive [2,9,10,16,27].

Many bone replacement substitutes such as polymethylmethacrylate (PMMA), hard tissue replacements, porous polyethylene, bioactive glass particulate, and hydroxyapatite (HA) have been used for cranial defect reconstructions. Each of these materials has advantages and limitations. A few of the bone replacement substitutes are briefly covered as per the information obtained from literature review.

2.2.1 Polymethylmethacrylate (PMMA)

Polymethylmethacrylate is an acrylic-based resin and is found to be stronger than adjacent skull bone to compression and torsion. It is resistant to absorption, low in cost, of predictable shape, easily available, and suitable for complex defects [2,27].

However, disadvantages are since it is an inert and fixed substance, it will not adapt to a changing cranial skeleton, especially in the case of a growing child. Additionally, no bone resorption or ingrowth occurs, as it is a non-porous material. It sets exothermically (high as 55^0C) and may lead to tissue necrosis of surrounding tissues [2,5,6,8,27,38].

2.2.2 Bioactive Glass Material

Bioactive materials cause a formation of a bond between the tissue and the material by a specific biological response at the interface of the material [2]. It is osteoconductive, and the interfacial bonding strength is equivalent to or greater than that of bone. Mechanical failure does not occur at the bone interface but at the host bone or within the biomaterial [2,13].

Disadvantages include complications during contour restoration and failure due to extrusion [13]. These materials lack initial strength as compared to other biomaterials because of their property of gaining strength following bone growth and incorporation [9,13].

2.2.3 Demineralised Bone

Demineralised bone material is a freeze-dried cortical demineralised powder with little tissue reaction and little osteoclastic activity. These materials are porous and can be easily molded to fit the defect. The material remains as a paste and does not harden [2,3,9,13]. Disadvantages of demineralised bone are that it is not well suited for load bearing regions since it will not harden to bear significant load and has a high resorption rate [2,3,13].

2.2.4 Hydroxyapatite

Hydroxyapatite (HA) is the most extensively used biomaterial for cranial defect reconstruction. Different forms of HA are available for clinical use. Each form behaves differently in its physical and biological behavior [10,23]. HA is shown to be an excellent biocompatible material that is radiolucent and readily available. Various authors have described it as having osteoconductive properties [2,8,10,14,17].

Hydroxyapatite is mainly available in ceramic, cement paste, and granular forms [2,17]. There are two types of HA in current clinical use, the macro porous with a pore size of 100 to 500µm, and the micro porous with a pore size of less than 10µm. Porous ceramic forms of hydroxyapatite have shown bone ingrowth when implanted in animal models. However, the ceramic form is difficult to mold intraoperatively, is brittle, and has low tensile strength [17]. Studies indicate more bone replacement in ceramic HA when compared to cement paste implants due to porosity of implants [1,2,6,17].

HA cement paste forms when tetracalcium phosphate and dicalcium phosphate mix in the presence of water. The two calcium salts undergo an isothermic reaction to form a dense paste that has been claimed to be resorbable over time. The setting time of the paste to harden is approximately 30 minutes. Modification by mixing the powder in a sodium phosphate buffer solution can accelerate the setting time of the cement from approximately 30 to 10 minutes [10]. Cement paste HA can be easily shaped during surgery [2,24]. HA cement has been extensively used for reconstruction of cranial defects.

Setting time for HA cement plays an important role. Hemostasis needs to be maintained while applying HA cement. The time between mixing and final setting of the HA cement is crucial. Balance must be achieved for working, molding, and operating time [10]. Fast setting HA cements are available which claim to set in approximately 5 minutes, reduce the operating time and operating room expense, and also achieve favorable results. Various authors suggest that less than 5 minutes of setting time is preferred [5,10].

Moriera et al. [27] described HA as initially promising, but follow-up after a few months showed adverse results. Inflammatory reactions with swelling, exposure, thinning of the skin envelope, pain, no bony ingrowth, and tissue reaction were associated with its use. The author suggested that a delayed immunoguided inflammatory reaction is possible with use of HA.

Carbonated calcium phosphate (CCPP) bone cement is another form of HA which is used on a widespread basis. It contains monocalcium phosphate, monohydrate, α-tricalcium phosphate and calcium carbonate. It mixes with sodium phosphate solution to form dahllite, by isothermic reaction. Dahllite contains carbonate content (4-6%), which is absent in other forms of HA. It has a molar calcium to phosphate ratio of 1.67:1 [31]. Dahllite is biocompatible and resembles the mineral component of bone [33]. CCPP is soluble at low pH and is a low order crystalline apatite [16,39]. The material is known for setting in less than 10 minutes and approximately 85-90% setting after 12 hours [31,39]. By changing the crystallinity of HA or particle size when in solid phase, the compressive strength of CCPP can be altered [31]. Some authors cite that CCPP remodeling is based on the osteogenic capacity of the host and composition of the implant. Their study shows results of better remodeling in skeletally immature animals as compared to mature animals [33].

2.2.5 Scaffold with HA Cement

During reconstruction of cranial defects, an underlying mesh is used to prevent the interference of crystallization of the cement with the underlying brain and dura [14]. Fragmentation of the implant occurs during the process of crystallization of the cement due to dural pulsations. Interposed bioresorbable or metallic plates or meshes are usually

used between the HA cement and the dura, which acts like a scaffold and dampens the pulsations experienced [1,13,14,36].

Titanium mesh is used as a scaffold with HA cement. It is thought to increase the durability of the reconstruction by maintaining its integrity and geometry during the time of healing. It is known that HA can be placed safely directly over dura. However, without the underlying mesh in situ, it becomes difficult to adjust the three-dimensional contour of the HA cement for critically sized defects. Titanium is biocompatible and corrosion resistant [7]. Although titanium mesh and HA cement reconstruction appears to be a reasonable method, its long-term ability to withstand trauma and biomechanical stability is unknown [7]. Some authors have cited that reconstruction with a mesh does not improve the impact resistance of the structure and only acts as a method to control setting of the material [10].

Tantalum mesh and titanium miniplates are suggested for use with HA cement for treating large cranial defects (greater than $25cm^2$) [8]. Bioresorbable polylactic acid [PLA] mesh is also used in cranial reconstructions with calcium phosphate. Resorbable meshes do not interfere with radiographic diagnosis [20,36].

CHAPTER III

MATERIALS AND METHODS

3.1 Reconstruction Materials

Sixty to seventy percent of dry bone weight is carbonated apatite. The reconstruction cements used in this study have a carbonated apatite content of 5%, and closely resemble bone when set [28,46].

Norian Craniofacial Repair System (CRS) (AO North America, Devon, PA) and Norian CRS Fast Set Putty are calcium phosphate-based bone cements approved for use in the repair of skull injuries *in vivo*. Both products are developed and manufactured by Norian Corporation and are distributed by Synthes Maxillofacial, USA. These bone cements are moldable, are compatible with body tissues, and set (harden) at body temperature. Key to their use in surgical applications and in this study is their ability, over time, to be resorbed by the body and replaced by bone. The main difference between these materials is the amount of time required for the cement to harden. Norian CRS requires approximately 10 minutes to set, whereas Norian CRS Fast Set Putty becomes usable in approximately 3 minutes [46].

In this study, the reconstruction structure of Norian CRS with titanium mesh scaffold is referred to as Reconstruction A (RCA) and that of Norian CRS Fast Set Putty with titanium mesh scaffold is referred to as Reconstruction B (RCB). To replicate autogenous bone grafts (ABG), a full thickness cranial defect from the parietal bone

of each sheep skull was measured and replaced as a full thickness bone graft on the contra lateral side of the parietal bone of sheep skull [28].

Titanium miniplates and screws from Synthes, CO, USA were used to fix the bone grafts (Figure 3.1). Titanium mesh used for the scaffold was a 1.5mm TI contourable mesh (Synthes, CO, USA).

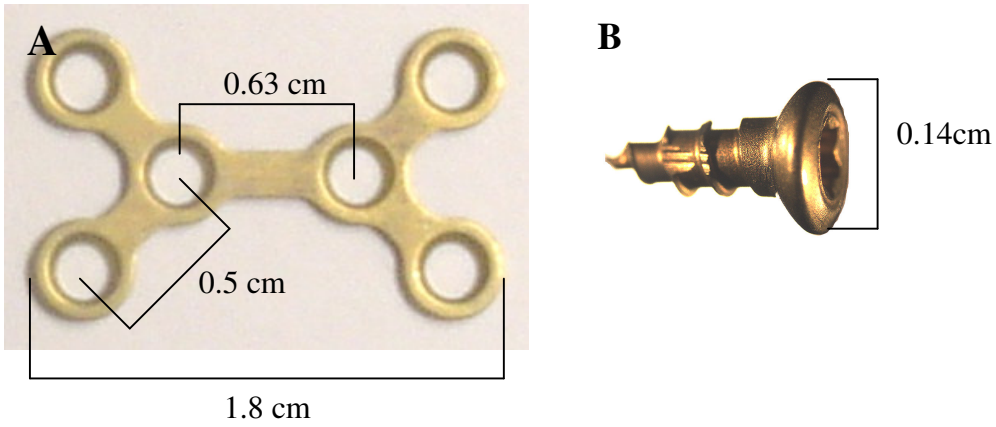

Figure 3.1. Titanium miniplate (A) and screw (B) used to secure scaffolding in skull reconstructions. Miniplate is shown at approximately 1.5 times actual size; screw is illustrated at approximately 5 times actual size.

3.2 Sources of Skull Material

Twenty-four skeletally mature female sheep (average 1 year old) served as sources of skull material. The skulls of these sheep were provided by the Cleveland Clinic Foundation for use in this investigation. Each animal underwent surgery prior to this investigation to create skull defects and place skull reconstructions. Depending on the assignment of the sheep to one of the eight groups, each animal received either an ABG, RCA, or RCB reconstruction (experimental groups), or no reconstruction (control group). The reconstructions were in place for three different time periods following

surgery: sheep in the t_0 group were sacrificed immediately after placement of the reconstruction, sheep in group t_1 retained the reconstruction for six months following placement, and sheep in group t_2 retained the reconstruction for twelve months postoperatively. Each sheep was euthanized prior to skull harvesting surgery.

3.3 Description of Critical Size Defects and Placement of Reconstructions

Unilateral or bilateral, rectangular, full thickness critical size defects measuring 1.5 × 3.0cm (4.5cm^2) were created in the parietal bone of the sheep skull (Figures 3.2 - 3.4) [28]. The defects were then reconstructed using either an autogenous bone graft

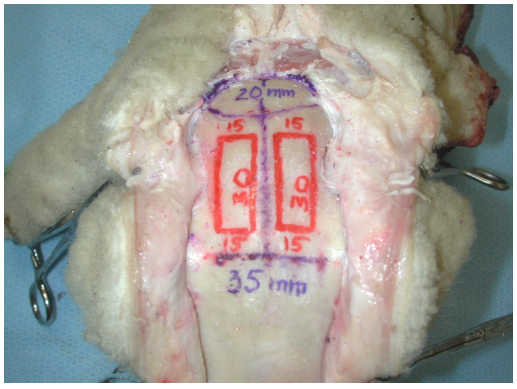

Figure 3.2. Marks on the epithelial surface of a sheep skull to show the size and placement of the simulated defects. Image courtesy of the Department of Plastic Surgery, Cleveland Clinic.

(Figure 3.5) or RCA or RCB - reconstruction techniques. The RCA or RCB reconstructions on the right side were secured with titanium mesh scaffolding and a titanium miniplate and screws (Figures 3.6 and 3.7). The open defects were sealed as shown in Figure 3.7.

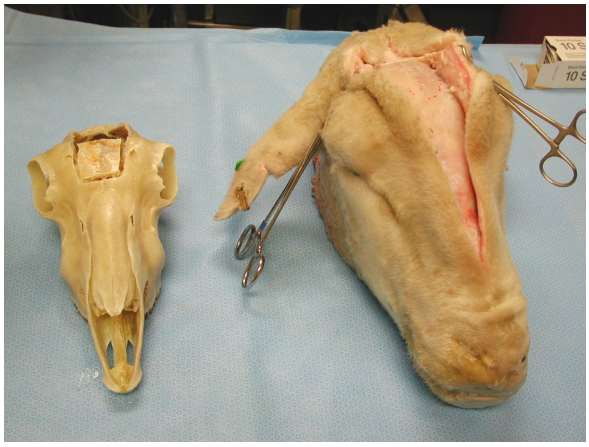

Figure 3.3. Defects in the parietal bone of a cleaned sheep skull, left, and a whole skull, right. Image courtesy of the Department of Plastic Surgery, Cleveland Clinic.

Figure 3.4. 4.5cm^2 full thickness cranial defect created in the sheep skull.

Figure 3.5. Full thickness cranial bone removed (right side) to be used as autogenous bone graft in the collateral side (left side).

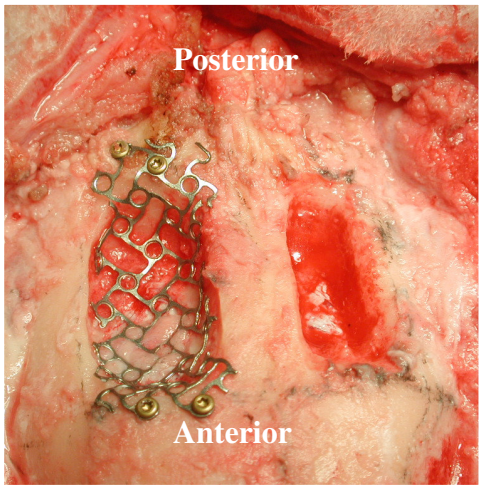

Figure 3.6. Bilateral defects created in the sheep skull. To the right is the defect created in the left side of the parietal bone; to the left is a similar defect in the right side of the parietal bone. The defect in the right parietal bone has been partially reconstructed with titanium mesh.

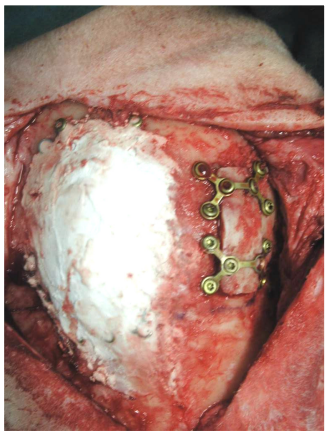

Figure 3.7. Sheep skull showing the reconstruction techniques completed. In this view, the autogenous bone graft has been placed in the defect in the right side of the parietal bone and the left defect sealed.

3.4 Classification of Samples

Initially, 24 skeletally mature female sheep (1 year old) were assigned to eight experimental groups. Skull samples were harvested at follow-up periods t_0 (0 month), t_1 (6 months) and t_2 (12 months). Two sheep had to be sacrificed due to complications and were replaced. In total, 24 samples were available to be experimentally tested. Six skulls with bilateral defects were tested at time t_0 and six skulls at t_1; twelve skulls with either bilateral or unilateral defects were tested at t_2. Assignment of reconstruction techniques to skulls in each group was alternated as indicated in Table 2.

Table 2. Assignment of sheep to experimental groups

Follow-up Period	Reconstruction Technique	Number of Samples
t_0	RCA (right) ABG (left)	3
	RCB (right) ABG (left)	3
t_1	RCA (right) ABG (left)	3
	RCB (right) ABG (left)	3
t_2	RCA (right) ABG (left)	3
	RCB (right) ABG (left)	3
	RCA (right) Intact (left)	3
	RCB (right) Intact (left)	3

3.5 Experimental Testing Apparatus

The human cranium undergoes linear fracture due to stresses near the site of impact. Drop weight tests, therefore, create situations of impact that allow measurement of impact structural resistance of the skull [10,23]. Drop weight testing simulates abrupt impacts to the skull, such as those experienced in certain types of head injury, including blunt force trauma and collision between the head and hard surfaces (such as pavement). Typically such impacts have duration of 5-40 milliseconds. Impact testing is one of the

criteria used for testing headgear (e.g., motorcycle helmets) by the U.S. Department of Transportation and the Snell Memorial Foundation [34,37].

In a drop weight test, a weight is dropped on the specimen from a specified height. Either the weight or the height can be held constant during testing sequences. In this study, the weight (mass) was held constant and height was varied. This was set via interaction between Department of Plastic Surgery, The Cleveland Clinic Foundation, Orthopaedic Research Laboratories, Dr. Glen Njus, and the literature review. Transmitted force, time, and acceleration of the mass were recorded for each test.

3.6 Experimental Procedure

Figure 3.8 illustrates an outline of the testing protocol followed in this study. Each component of the protocol is described in greater detail in the remaining sections of this chapter.

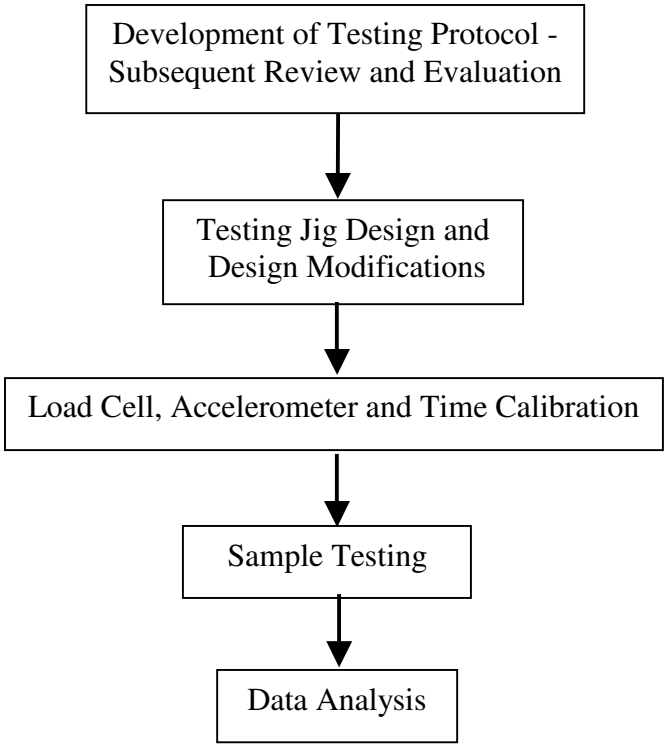

Figure 3.8. Flowchart outlining the experimental protocol.

3.6.1 Testing Protocol

The samples were tested based on their follow-up period. Samples of t_0 were tested initially, followed by t_1 and t_2 samples. Since the defects in the sheep skulls were in close proximity to one another, the right side of all samples (RCA / RCB) was tested first followed with the left side (ABG and Intact bone) of the specimen. This decision was made to avoid any effect of the drop weight test on the results of RCA / RCB. The testing protocol was written and carried out as explained in the samples testing section 3.6.4 below. Specifications for the drop weight tests are described in Appendix B.

3.6.2 Development of Jig

Skull samples showed some variability in their overall dimensions, so it was necessary to develop a jig that would allow each specimen to be held in a stable adjustable plane. Figures 3.9 and 3.10 depict the variability in sheep skull samples.

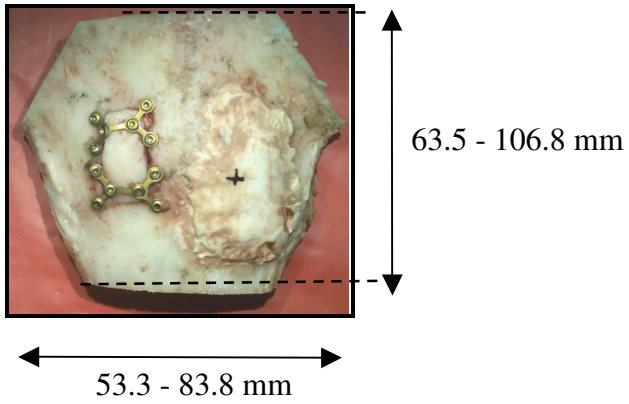

Figure 3.9. Epithelial (top) surface of a sheep skull, showing side-by-side defects. Range values indicate variability in overall dimensions of skulls.

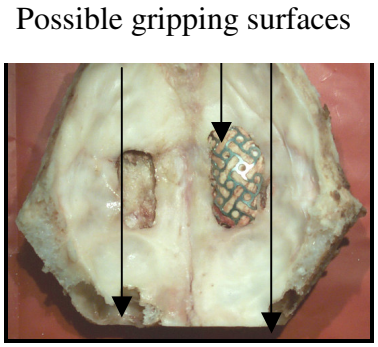

Figure 3.10. Epidural surface (underside) of a sheep skull showing the location of surfaces that rest upon the apparatus during testing. Variation between skulls required that the testing jig be adjustable to account for differences in these surfaces.

The impact system was designed so that the sheep skulls could be held in a stable adjustable plane by adjustable neoprene balls, which provided points of contact with the epidural surface of each skull sample. Modifications made were so that x, y and z translations could occur. Figures 3.11 and 3.12 illustrate the jig system devised to hold the skulls in position for impact testing.

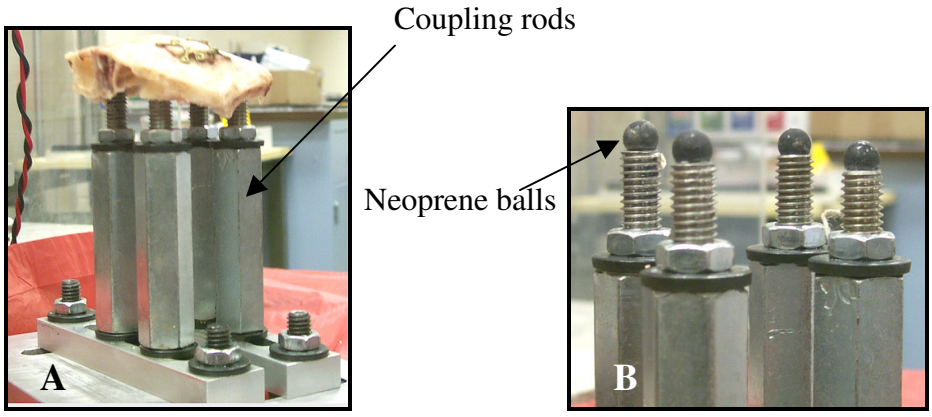

Figure 3.11. Jig system used to hold skulls in position (A) and close-up of adjustable contact surface. Each rod supporting a neoprene ball could be adjusted up or down to conform to the contours of the skull.

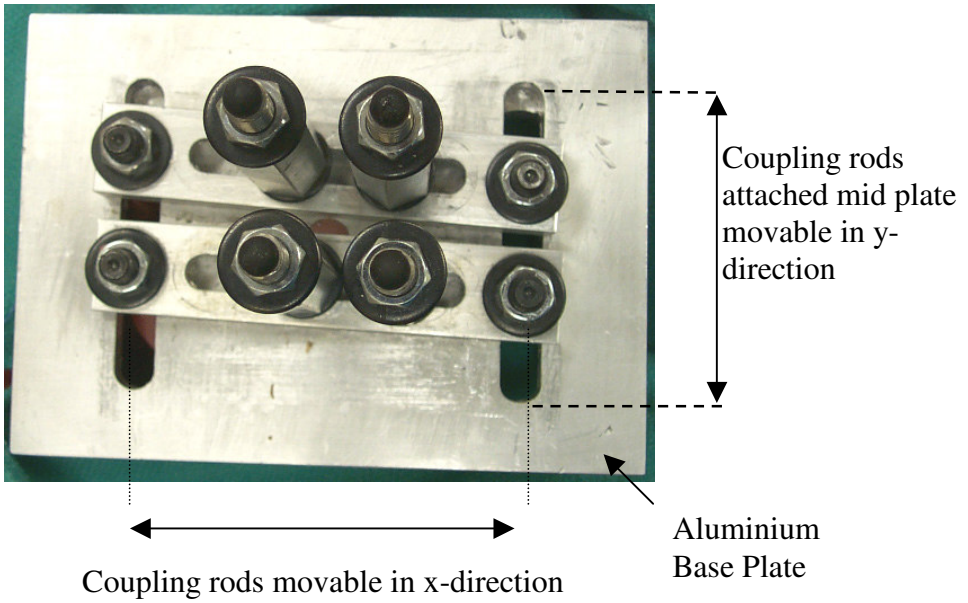

Figure 3.12. View from above the jig showing the axes of movement of the coupling rods. Rods could be moved to allow the jig to conform to the contours of the sheep skull.

Neoprene balls attached to the coupling rods provided a compliant contact surface to rest the base of the sheep skulls and avoid direct steel bone interfaces. This entire fixture was attached at its base (aluminium) plate to a ground reference load cell. Specification of the aluminium base plate of the jig is described in Appendix D.

3.6.3 Load Cell and Accelerometer Calibration

Before conducting drop weight tests on the sheep skulls, load cells and the accelerometer were calibrated. Calibration of the load cell was conducted by placing weights of known masses on the apparatus and observing voltmeter readings generated. Load cell function was tested by pressing down on the cell by hand and ascertaining that the compression caused a change in the voltmeter reading. Calibration of the

accelerometer was conducted by drop test of known height of 5.08 cm and 10.16 cm. During testing, accelerometer was balanced using the auto balance routine. The load cell and accelerometer were calibrated prior to each test.

3.6.4 Preparation of Samples for Testing and Testing Process

The testing area was prepared by placing bio-hazard polymer sheeting below the drop device to prevent contamination. Each of the neoprene balls was checked to make sure it was secure on its coupling rod; any loose neoprene balls were reattached using either epoxy or cyanoacrylate. Each sheep skull specimen was defrosted and kept in a beaker of 0.9% Ringers solution while the apparatus was prepared and calibrated. The point of impact for the side of the skull to be tested was marked at the center of the reconstruction on the specimen to be tested. The center point was located using a vernier caliper.

An indenter was attached rigidly to the spherical drop mass, and indenter weight and length were noted prior to each test. The spherical drop mass with attached indenter was placed on an electromagnet, which held the mass in place above the jig and skull sample. The specimen to be tested was placed on the jig, and the indenter aligned with the point of impact marked on the skull. Alignment of the indenter was accomplished by using a plumb bob, suspended between the tip of the indenter and the skull. A bubble level was used to ensure that the skull was level, and the coupling rods were adjusted as necessary to achieve level. Figure 3.13 shows the entire apparatus with the skull specimen in place prior to a drop weight test.

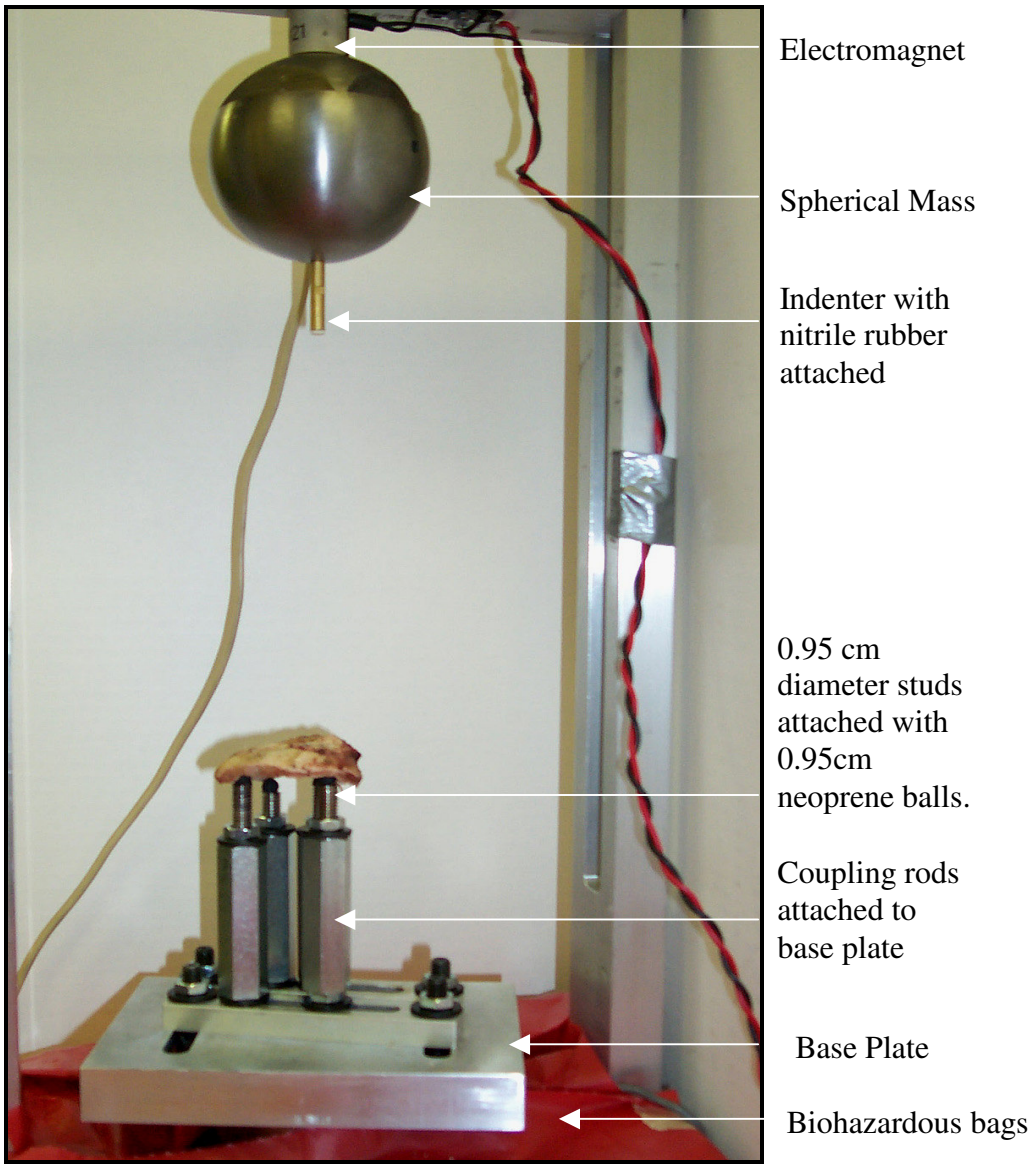

Figure 3.13. Drop weight test apparatus. Note the position of the skull sample on the coupling rods and its position relative to the indenter and spherical mass.

The indenter was covered with nitrile rubber to simulate the surface of the skin; the nitrile rubber was attached to the indenter with double-sided tape. The distance between the tip of the indenter and the skull was measured with an acrylic rod that was cut to a predefined length, ensuring that the reconstructions would break in one impact

(Figure 3.14). While the indenter was adjusted and aligned, the skull specimens were kept moist by placing gauze pieces soaked in Ringers solution on the skulls; the gauze was removed before each test, and surgical drapes were placed below the specimen to prevent any of the solution from dripping into the test apparatus.

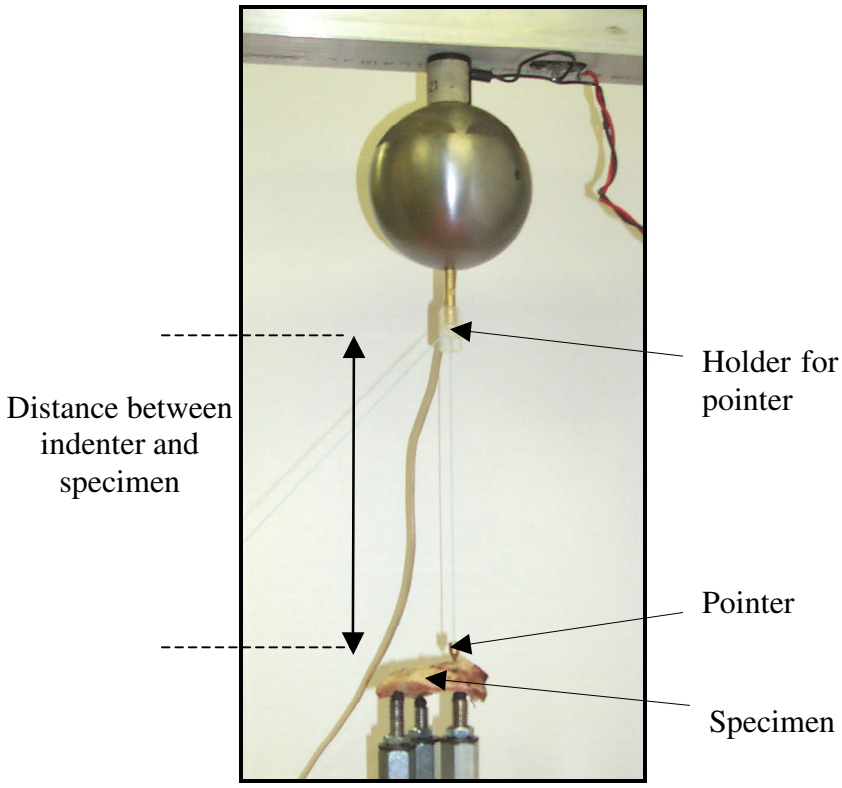

Figure 3.14. Test apparatus showing the height measurement and pointer marking.

An example of the data recording interface is shown in Figure 3.15. Data were collected for 2 seconds with a sampling frequency of 4000 Hz, thus allowing sufficient time and sensitivity to record data from 5-40 millisecond impacts. To begin data collection, the software was initialized, and the "start" button was clicked. Clicking the "start" button triggered the on/off switch of the electromagnet, setting it to "off", thus releasing the drop weight. The data were saved by pressing File and the Save button.

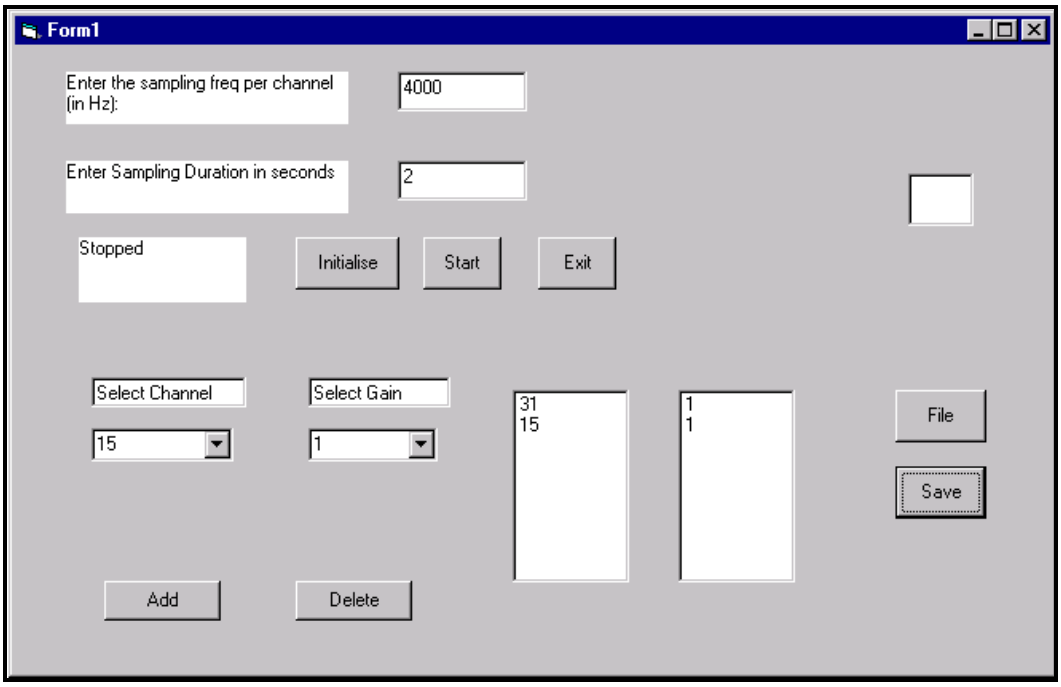

Figure 3.15. Data recording interface showing data collection.

Immediately after each drop test, the specimen was removed carefully from the jig and pictures were taken of the specimen and the jig from various positions as needed. The specimen was not placed back in saline solution during the repeat testing protocol but was kept hydrated by placing a 2x2 piece of gauze soaked in Ringers solution on the specimen until the next trial. The entire procedure was repeated for the remaining half of each skull sample. When testing was completed, each specimen was placed in a container of formaldehyde solution and stored for histological analysis.

3.6.5 Data Analysis

An example of the data analyzed using Microsoft ® Excel 2000 is found in Figure 3.16. These curves were for the right side of an RCB specimen at t_1 (6 months) period (animal code BO 5285, group 1B). The y-axis of the upper graph has units of accelerations due to gravity and was measured with an accelerometer. In the SI system 1 g = 9.802 m/s^2; where 'm' stands for meter, and 's' stands for second.

Figure 3.16 depicts the results of a drop weight test in which a load cell was fixed to ground on the far side of the specimen. Note that the start of the two curves and peaks are offset with respect to time a few tenths of a millisecond.

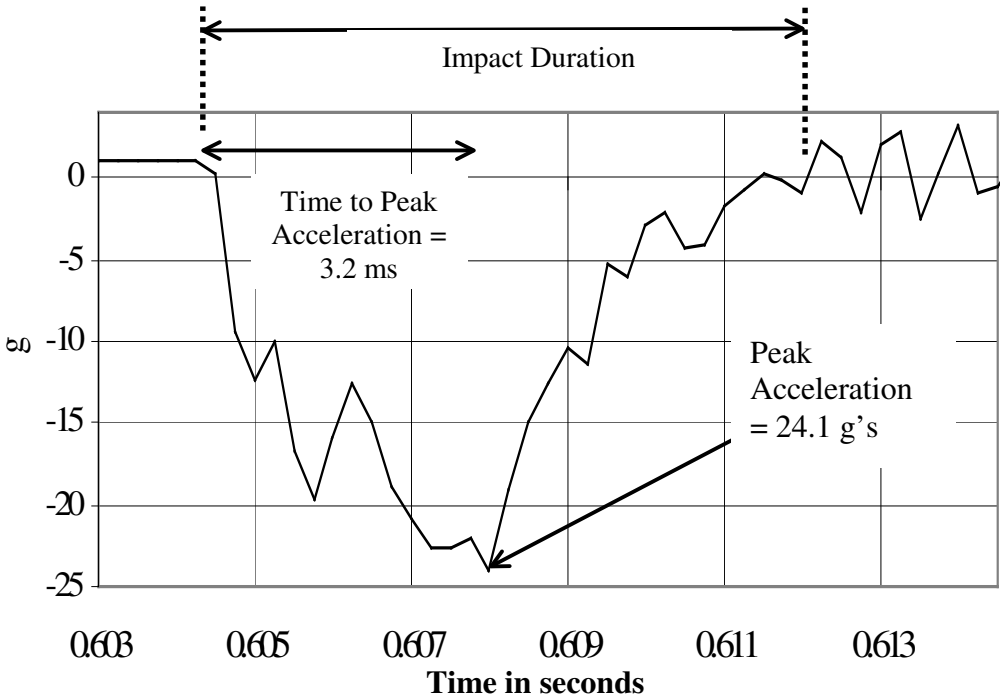

Figure 3.16. Graphical representation of data from a typical drop weight test in which a load cell was fixed to ground on the far side of the specimen.

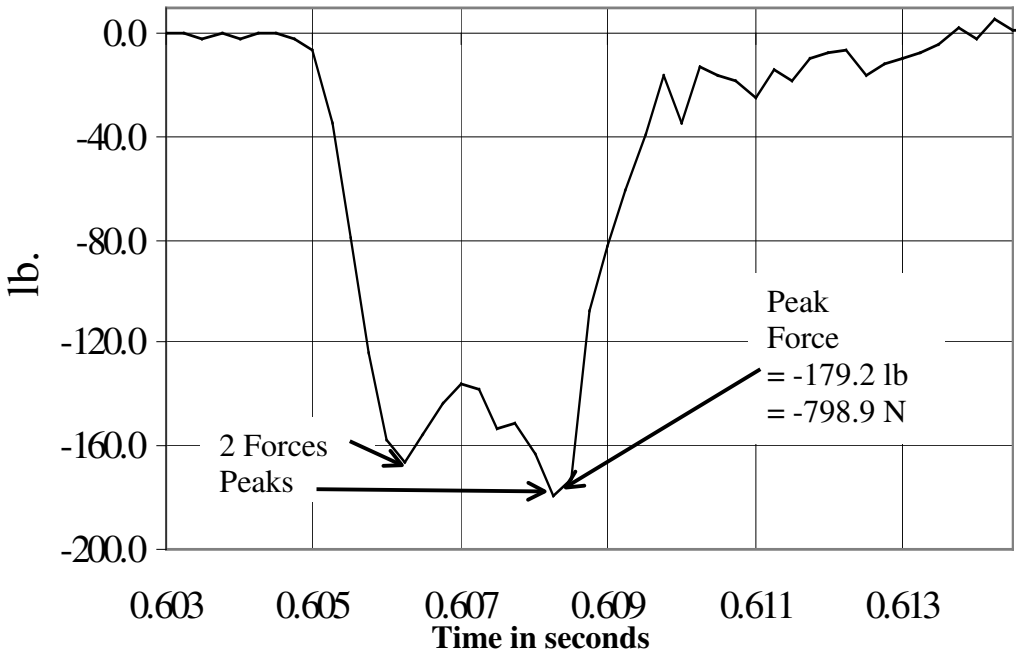

Figure 3.16. Graphical representation of data from a typical drop weight test in which a load cell was fixed to ground on the far side of the specimen (contd).

The following parameters were measured during each drop weight test:

1. Peak Acceleration: Maximum negative acceleration of the impacting anvil, recorded in g's, which gave the force required to fracture the cranial reconstruction. This is the most important parameter recorded in this study as described in section 5.1

2. Peak Force Transmission: Maximum force recorded by load cell, in newtons (N), which gave the energy absorption of the reconstruction during fracture.

3. Time to Peak Acceleration: Rise time to achieve peak acceleration from the start of impact, in milliseconds as shown in Figure 3.16.

4. Impact Duration: Time required from start to completion of impact, in milliseconds.

5. Impulse to Peak Acceleration: Energy absorption calculated in N-sec from start of impact to peak acceleration.

6. Impulse during Duration: Energy absorption calculated in N-sec during the entire event. The parameters related to impulse were not considered for statistical analysis as described in section 4.3.

7. Displacement to Peak Acceleration: Displacement at the impact region of the skull calculated in mm from start of impact to peak acceleration.

8. Displacement to Impact Duration: Displacement at the impact region of the skull calculated in mm for the entire event. The parameters related to displacement were not considered for statistical analysis as described in section 4.3.

9. No of Acceleration & Force Peaks: The number of acceleration and force peaks recorded during the impact event. In some specimens, the number of acceleration peaks or force peaks is more than one (Figure 3.16), which could be due to indenter sliding, double impact.

10. Height: The distance between the tip of the indenter and the specimen surface, calculated in cm from the data obtained. The height was increased from 19cm to 42cm in between tests as shown in Figure 5.3.

Data reports were produced in tabular form for each drop weight test. Figure 3.17 depicts a typical data table reported for an individual test. Likewise, Figure 3.18 illustrates the tabular report of the data on velocity and impulse during a drop weight test.

Time **(t)** (sec.)	Force (N)	Acc. **(a)** (g's)	Time (sec.)	Force (N)	Acc. (g's)
0.60300	-1.1	1.0	0.60875	-479.8	-12.6
0.60325	-1.1	1.0	0.60900	-367.0	-10.4
0.60350	-6.6	1.0	0.60925	-267.9	-11.4
0.60375	-1.1	1.0	0.60950	-174.4	-5.2
0.60400	-6.6	0.9	0.60975	-72.6	-6.0
0.60425	1.7	0.9	0.61000	-155.1	-2.8
0.60450	-1.1	0.3	0.61025	-58.8	-2.2
0.60475	-6.6	-9.5	0.61050	-69.8	-4.4
0.60500	-25.8	-12.3	0.61075	-80.8	-4.1
0.60525	-152.4	-10.0	0.61100	-108.4	-1.8
0.60550	-353.2	-16.8	0.61125	-64.3	-0.8
0.60575	-551.3	-19.7	0.61150	-80.8	0.3
0.60600	-699.8	-16.0	0.61175	-42.3	-0.2
0.60625	-741.1	-12.6	0.61200	-34.1	-0.9
0.60650	-691.6	-14.9	**0.61225**	**-25.8**	**2.2**
0.60675	-639.3	-18.9	0.61250	-69.8	1.3
0.60700	-603.5	-20.9	0.61275	-50.6	-2.1
0.60725	-611.8	-22.7	0.61300	-42.3	1.9
0.60750	-683.3	-22.6	0.61325	-31.3	2.7
0.60775	-669.6	-22.0	0.61350	-20.3	-2.5
0.60800	-724.6	**-24.1**	0.61375	9.9	0.3
0.60825	**-798.9**	-19.0	0.61400	-6.6	3.3
0.60850	-768.6	-15.0			

Figure 3.17. Data report generated by a typical drop weight test on the right side of a t_1 specimen (animal code BO 5285, group 1B). Shaded box in the third column indicates the beginning of the impact event; the shaded box in the sixth column indicates the end of the impact event.

Time (sec.)	Velocity (v) (m/s)	Displacement from Release (d) (m)	Impulse (N-sec.)	Time (sec.)	Velocity (m/s)	Displacement from Release (m)	Impulse (N-sec.)
0.60300	2.8747	0.4245		0.60875	2.1942	0.4398	-2.2394
0.60325	2.8772	0.4252		0.60900	2.1659	0.4403	-2.3305
0.60350	2.8797	0.4259		0.60925	2.1391	0.4409	-2.4169
0.60375	2.8822	0.4266		0.60950	2.1188	0.4414	-2.4827
0.60400	2.8846	0.4274		0.60975	2.1051	0.4419	-2.5269
0.60425	2.8869	0.4281		0.61000	2.0943	0.4424	-2.5617
0.60450	2.8884	0.4288		0.61025	2.0882	0.4430	-2.5814
0.60475	2.8770	0.4295	-0.0365	0.61050	2.0802	0.4435	-2.6072
0.60500	2.8503	0.4302	-0.1228	0.61075	2.0698	0.4440	-2.6408
0.60525	2.8230	0.4310	-0.2109	0.61100	2.0625	0.4445	-2.6642
0.60550	2.7902	0.4317	-0.3167	0.61125	2.0593	0.4450	-2.6744
0.60575	2.7454	0.4323	-0.4611	0.61150	2.0587	0.4456	-2.6764
0.60600	2.7016	0.4330	-0.6023	0.61175	2.0588	0.4461	-2.6760
0.60625	2.6665	0.4337	-0.7156	0.61200	2.0575	0.4466	-2.6804
0.60650	2.6329	0.4344	-0.8242	0.61225	2.0590	0.4471	-2.6754
0.60675	2.5914	0.4350	-0.9578	0.61250	2.0633	0.4476	-2.6617
0.60700	2.5426	0.4357	-1.1153	0.61275	2.0622	0.4481	-2.6651
0.60725	2.4892	0.4363	-1.2876	0.61300	2.0620	0.4486	-2.6657
0.60750	2.4337	0.4369	-1.4668	0.61325	2.0678	0.4492	-2.6472
0.60775	2.3790	0.4375	-1.6431	0.61350	2.0681	0.4497	-2.6462
0.60800	2.3226	0.4381	-1.8252	0.61375	2.0654	0.4502	-2.6549
0.60825	2.2697	0.4387	-1.9957	0.61400	2.0698	0.4507	-2.6408
0.60850	2.2280	0.4392	-2.1303				

Figure 3.18. Tabular data report reporting velocity, displacement, and distance from release for a typical drop weight test. Shaded cell indicates the start of the impact event.

The velocity, displacement and impulse was calculated using the following mathematical formulas:

$$\text{Velocity} = \int a \bullet dt$$

$$\text{Displacement} = \int v \bullet dt$$

$$\text{Linear Impulse} = \int F \bullet dt = \int ma \bullet dt = m \int a \bullet dt = 3.222 \int a \bullet dt$$

3.6.6 Statistical Analysis

Since the study consisted of the Intact bone (control group) in the t_2 period, the statistical analysis was broken down to two cases to analyze the control group separately.

Case 1: Multivariate Analysis of Variance (MANOVA) was performed using the SAS® system for windows (release 8.02 TS level02MO), SAS Institute Inc., Cary, NC, USA, to determine whether any significant differences exist between the reconstruction techniques RCA / RCB / ABG (reconstruct) and their follow-up period (month) including any interaction effect between the reconstruct and month. If the interaction effect between the reconstruct and month for various parameters were significantly different, lsmeans output (in SAS) was used. Multiple comparison Student-Newman Keul's (SNK tests) were used when the null hypotheses were rejected for either reconstruction techniques or follow-up periods only (interaction between reconstruct and months showed no significant difference), to find out where the differences exist [29,35].

Case 2: MANOVA was performed to determine significant differences between the reconstruction techniques and intact bone (control group) tested for t_2 follow-up period. Dunnett's test was used in MANOVA to compare the reconstruction techniques to the control group [29,35].

CHAPTER IV

RESULTS

4.1 Specimen Testing

Of the 24 samples tested, drop weight tests were conducted for 22 samples. Two samples were sent directly for histological analysis. For some specimens, the skull completely fractured while testing one side; hence, both sides could not be tested.

4.2 Comparison of Results in Graphical and Tabular Format for the Sheep Skull Samples Analyzed

The drop weight test parameters were converted to graphical format for qualitative data analysis. The mean impact duration in milliseconds decreased for t_1 (8.6±1.8ms) and t_2 (6.7±2.4ms) follow-up period compared to t_0 (13.7±1.5ms) for RCA as shown in Figure 4.1. Figure 4.2 shows the time to peak acceleration in milliseconds from the start of impact to peak acceleration. At t_0 the time to peak acceleration for ABG was relatively high (4.0±1.4ms) compared to RCA (2.8±0.7ms) and RCB (2.7±0.5ms). Peak acceleration for RCA at t_0 (29±4.5g) decreased at t_1 (16.4±13.0g) and t_2 (18.2±9.1g) as shown in Figure 4.3. However, peak acceleration for RCB and ABG increased over t_1 and t_2. This indicates that RCA biomechanical properties decreased over a period of time, whereas RCB and ABG increased. Peak force transmission for RCA at t_0 (904±265N) was relatively high compared to t_1 (461±406N) and t_2 (613±251N)

follow-up period as shown in Figure 4.4. ABG peak force transmission increased over time, t_0 (928±321N), t_1 (1908±514N), and t_2 (3542±876N). The results were comparable to the peak acceleration findings that RCA properties decreased over time, whereas those of RCB and ABG increased. Figure 4.5 and Figure 4.6 show the impulse to peak acceleration and impulse during duration for RCA, RCB, ABG and intact bone over time, respectively. Displacement to peak acceleration for RCA at t_2 (10.59±1.70mm) was relatively high compared to RCB at t_2 (5.35±1.59mm) and ABG at t_2 (6.80±1.24mm) as shown in Figure 4.7. Data for the drop weight test of all the parameters along with the code assigned for each specimen, number of acceleration peaks, number of force peaks, and the effect of each drop weight test (comments) are shown in Table 3.

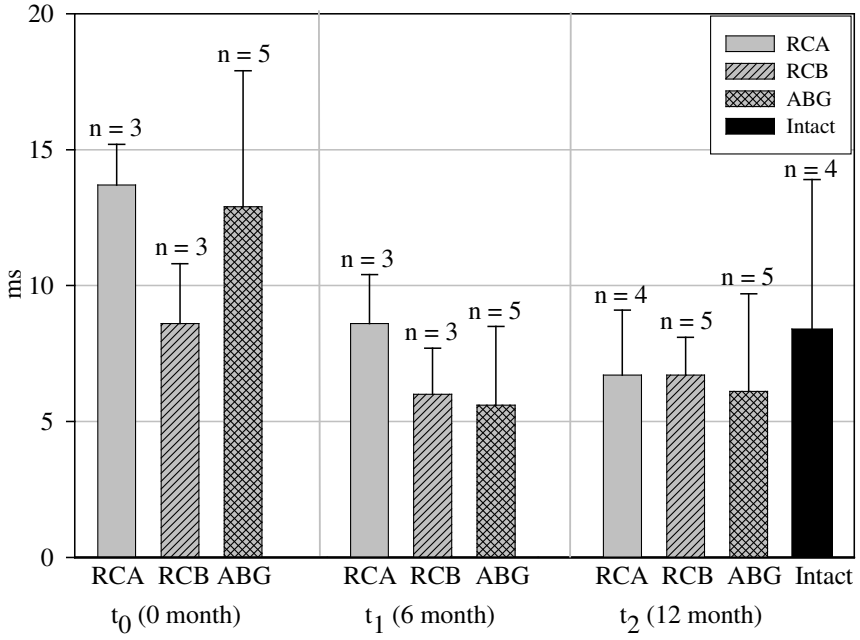

Figure 4.1. Impact Duration in millisecond of RCA, RCB, ABG and Intact bone for t_0,t_1 and t_2 follow-up period

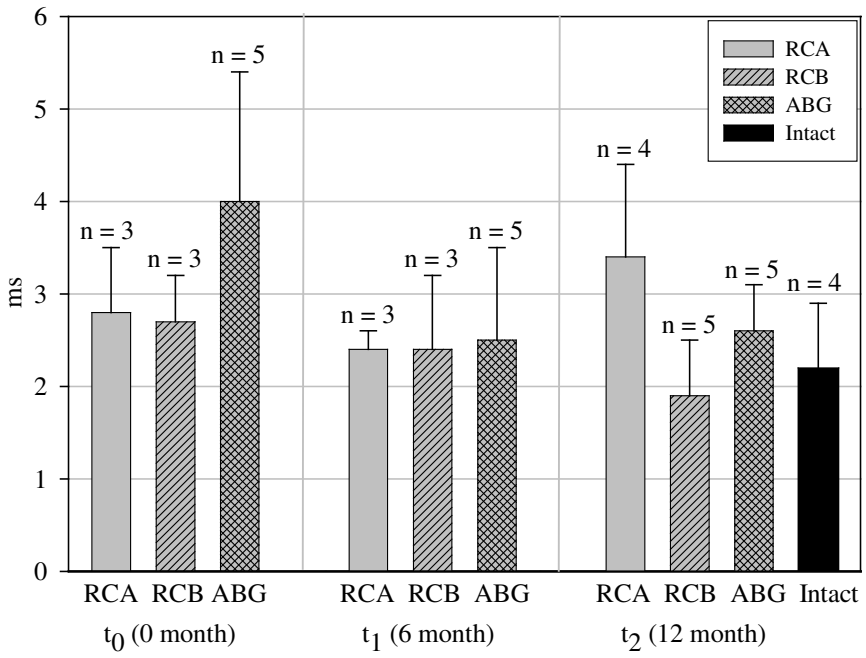

Figure 4.2. Time to Peak Acceleration in millisecond of RCA, RCB, ABG and Intact bone for t_0, t_1 and t_2 follow-up period

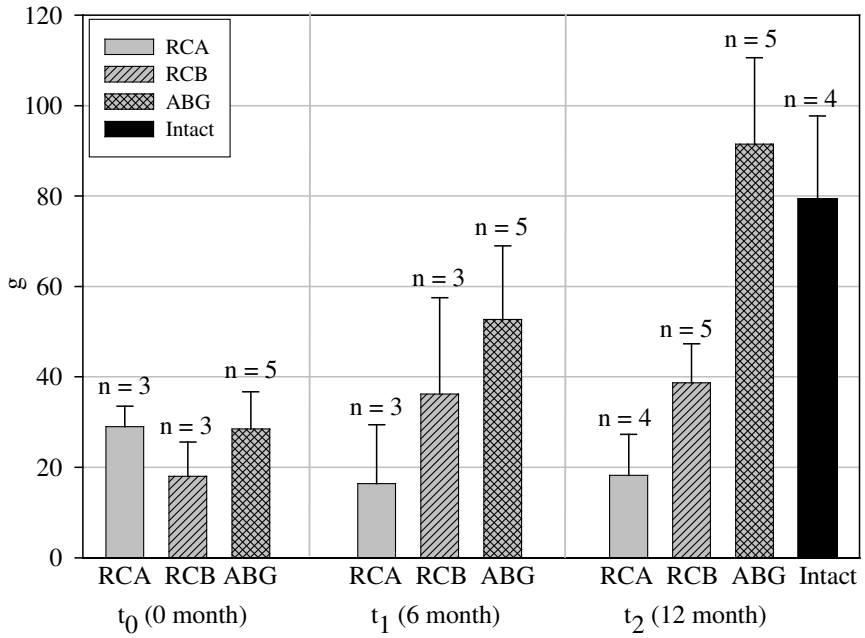

Figure 4.3. Peak Acceleration in g of RCA, RCB, ABG and Intact bone for t_0, t_1 and t_2 follow-up period

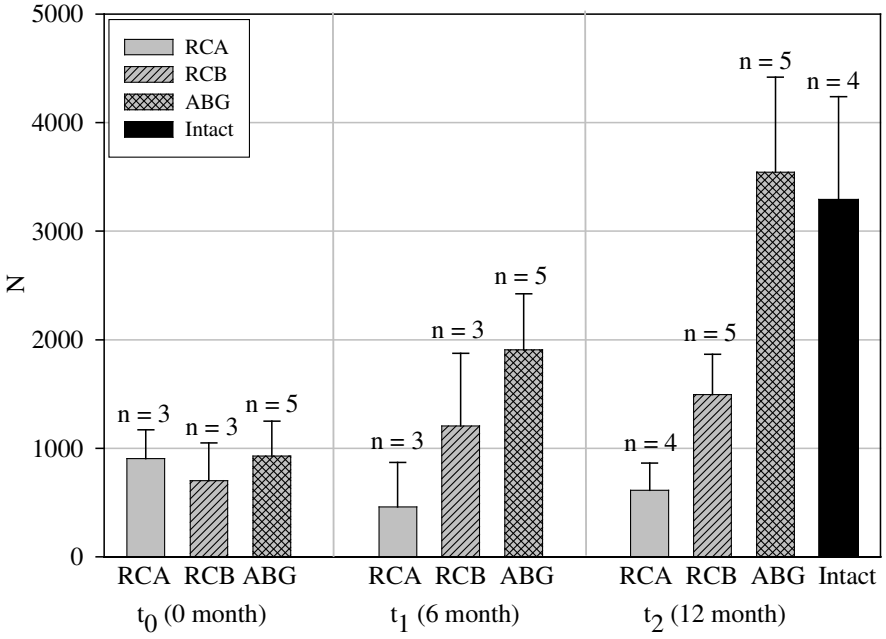

Figure 4.4. Peak Force Transmission in newton of RCA, RCB, ABG and Intact bone for t_0, t_1 and t_2 follow-up period

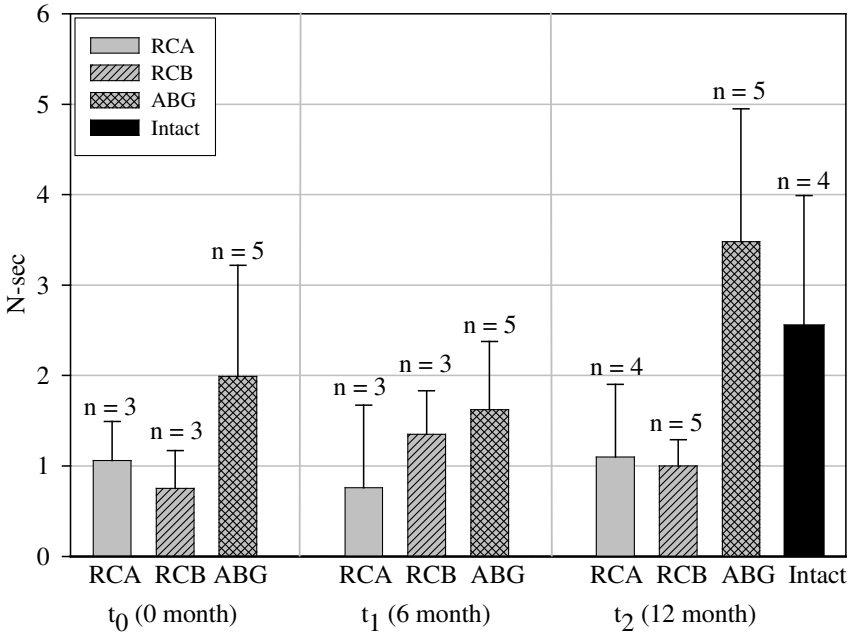

Figure 4.5. Impulse to Peak Acceleration in N-sec of RCA, RCB, ABG and Intact bone for t_0, t_1 and t_2 follow-up period

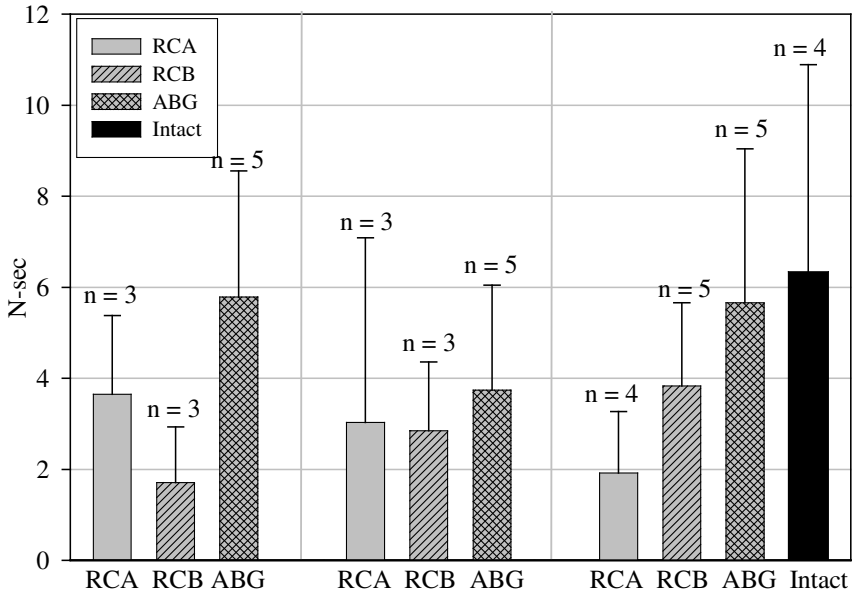

Figure 4.6. Impulse during duration in N-sec of RCA, RCB, ABG and Intact bone for t_0, t_1 and t_2 follow-up period

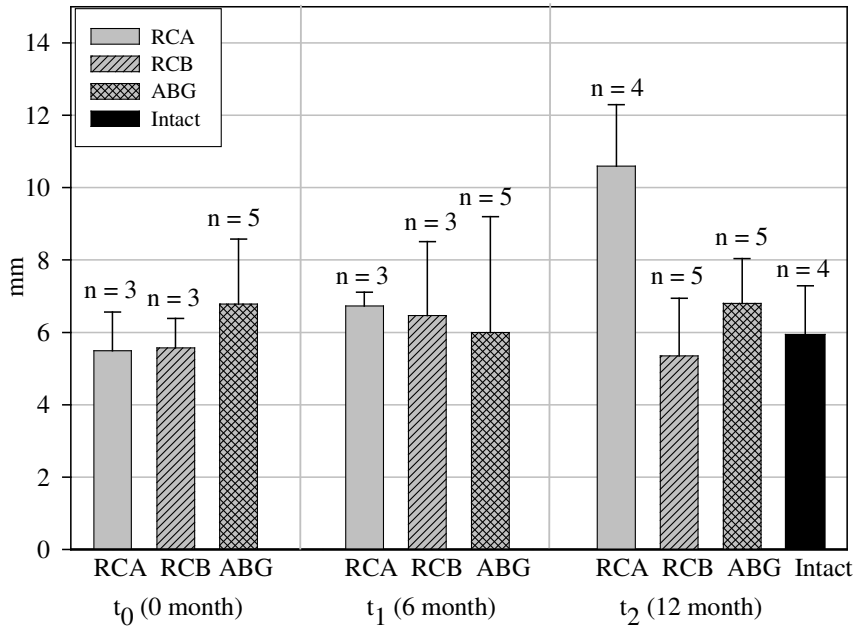

Figure 4.7. Displacement to Peak Acceleration in mm of RCA, RCB, ABG and Intact bone for t_0, t_1 and t_2 follow-up period

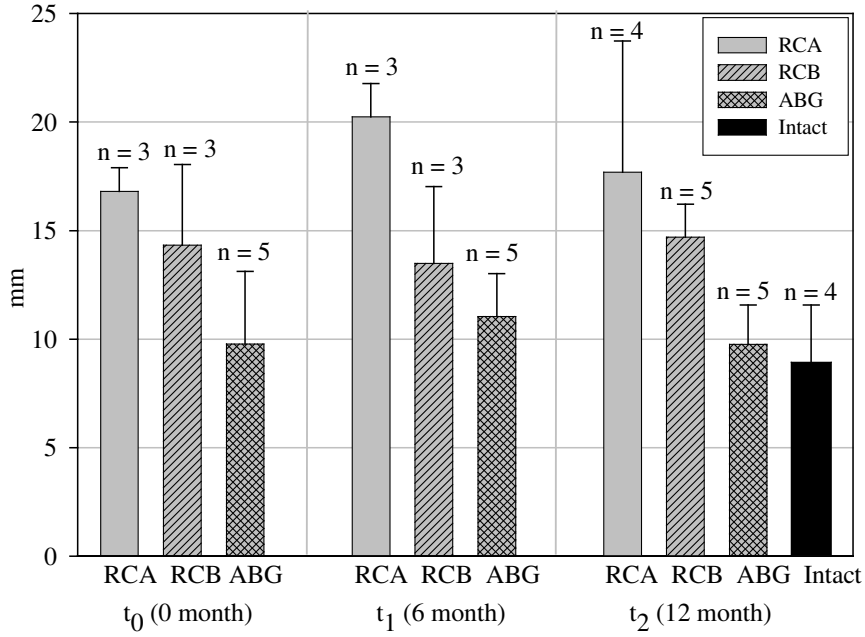

Figure 4.8. Displacement to impact duration in mm of RCA, RCB, ABG and Intact bone for t_0, t_1 and t_2 follow-up period

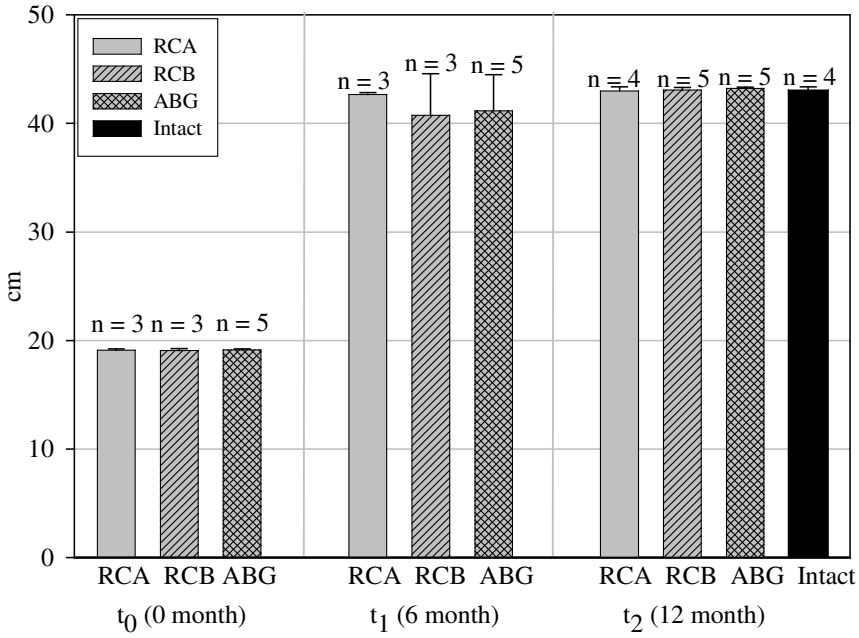

Figure 4.9. Height in cm between the indenter and specimen of RCA, RCB, ABG and Intact bone for t_0, t_1 and t_2 follow-up period

Table 3: Results of Drop Weight Test in Tabular Format

Code	Tech[1].	Imp[2]. Dur. (ms)	Time Peak Acc. (ms)	Peak Acc. (g)	Peak Force Trans. (N)	Ips[3]. Peak Acc. (N.sec)	Ips. of Dur. (N.sec)	Disp. Peak Acc. (mm)	Disp. Imp. Dur. (mm)	Acc. Peaks	Force Peaks	Ht[4]. (cm)
t_0-1	RCA	15.0	2.3	23.8	599	0.65	5.58	4.70	15.66	3	2	19.05
t_0-2	RCA	14.0	3.5	31.3	1065	1.51	3.12	6.71	17.80	1	1	19.01
t_0-3	RCA	12.0	2.5	32.0	1049	1.01	2.24	5.07	16.96	1	1	19.22
Mean		13.7	2.8	29.0	904	1.06	3.65	5.49	16.81			19.10
St. Dev.		1.5	0.7	4.5	265	0.43	1.73	1.07	1.08			0.11
t_0-4	RCB	8.0	3.2	26.4	1070	1.23	3.08	6.34	11.87	1	1	18.93
t_0-5	RCB	11.0	2.2	16.0	657	0.49	1.29	4.71	18.59	1	1	19.02
t_0-6	RCB	6.7	2.7	11.5	378	0.52	0.76	5.67	12.52	1	1	19.26
Mean		8.6	2.7	18.0	702	0.75	1.71	5.57	14.33			19.08
St. Dev.		2.2	0.5	7.6	348	0.42	1.22	0.82	3.71			0.17
t_0-7	ABG	14.7	2.2	23.9	833	0.65	5.60	4.21	15.15	2	2	19.06
t_0-8	ABG	4.5	3.5	16.1	458	0.97	1.20	6.40	8.00	1	1	19.08
t_0-9	ABG	17.5	6.0	34.2	1264	3.67	8.21	9.25	6.38	1	1	19.14
t_0-10	ABG	15.0	4.0	34.2	897	2.06	7.66	6.97	8.94	1	1	19.11
t_0-11	ABG	12.7	4.2	34.0	1188	2.59	6.29	7.09	10.36	1	1	19.25
Mean		12.9	4.0	28.5	928	1.99	5.79	6.78	9.77			19.13
St. Dev.		5.0	1.4	8.2	321	1.23	2.77	1.80	3.34			0.08
t_1-1	RCA	7.5	2.5	6.8	190	0.22	0.33	7.16	21.10	1	1	42.43
t_1-2	RCA	7.7	2.2	11.2	261	0.26	1.05	6.44	21.16	1	1	42.76
t_1-3	RCA	10.7	2.5	31.2	931	1.81	7.70	6.60	18.47	2	2	42.76
Mean		8.6	2.4	16.4	461	0.76	3.03	6.73	20.24			42.65
St. Dev.		1.8	0.2	13.0	409	0.91	4.06	0.38	1.53			0.19

Tech[1]: Technique.
Imp[2]: Impact.
Ips[3]: Impulse.
Ht[4] : Height

Table 3: Results of Drop Weight Test in Tabular Format (contd.)

Code	Tech[1].	Imp[2]. Dur. (ms)	Time Peak Acc. (ms)	Peak Acc. (g)	Peak Force Trans. (N)	Ips[3]. Peak Acc. (N.sec)	Ips. of Dur. (N.sec)	Disp. Peak Acc. (mm)	Disp. Imp. Dur. (mm)	Acc. Peaks	Force Peaks	Ht[4]. (cm)
t_1-4*	RCB	12.0	4.5	26.1	813	2.00	4.82	10.90	21.86	1	1	36.23
t_1-4*	RCB	10.2	4.2	52.7	1657	3.47	7.38	9.51	14.25	1	1	34.73
t_1-4*	RCB	12.0	4.2	47.9	1664	2.45	7.50	7.81	8.39	1	1	19.30
t_1-4	RCB	6.2	1.7	60.8	1975	1.36	4.44	4.46	11.45	1	1	36.33
t_1-5	RCB	4.2	2.2	23.7	846	0.87	1.43	6.37	11.42	1	1	43.04
t_1-6	RCB	7.5	3.2	24.1	799	1.83	2.68	8.56	17.57	2	2	42.88
Mean		6.0	2.4	36.2	1207	1.35	2.85	6.46	13.48			40.75
St. Dev.		1.7	0.8	21.3	666	0.48	1.51	2.05	3.54			3.83
t_1-7*	ABG	7.7	1.7	42.8	1317	1.43	5.80	4.31	12.67	1	1	35.16
t_1-8*	ABG	8.7	3.5	19.1	815	1.49	3.39	9.42	20.39	2	1	43.23
t_1-7	ABG	10.7	1.5	55.3	1960	1.44	6.92	3.65	13.15	2	1	35.26
t_1-8	ABG	5.0	2.7	55.6	2444	2.88	5.30	6.96	10.40	1	1	42.12
t_1-9	ABG	4.0	1.5	47.7	1326	1.26	2.34	4.12	9.76	1	1	42.74
t_1-10	ABG	3.7	2.7	75.0	2368	1.64	2.86	4.06	8.80	1	1	42.84
t_1-11	ABG	4.7	4.0	29.8	1442	0.90	1.28	11.19	13.09	2	2	42.87
Mean		5.6	2.5	52.7	1908	1.62	3.74	6.00	11.04			41.17
St. Dev.		2.9	1.0	16.3	514	0.75	2.31	3.19	1.98			3.32
t_2-1	RCA	9	4.25	7	291	0.31	1.01	13.01	25.97	2	1	43.25
t_2-2	RCA	8.5	3.5	28.7	853	2.21	3.92	9.15	18.28	1	1	42.65
t_2-3	RCA	4.25	2	16.1	544	0.90	1.29	9.78	12.36	1	1	43.37
t_2-4	RCA	5.2	3.7	20.8	763	0.98	1.45	10.40	14.13	1	1	42.66
Mean		6.7	3.4	18.2	613	1.10	1.92	10.59	17.68			42.98
St. Dev.		2.4	1.0	9.1	251	0.80	1.35	1.70	6.06			0.38

Tech[1]: Technique.
Imp[2]: Impact.
Ips[3]: Impulse.
Ht[4] : Height
*: Tests were conducted again to obtain desired output.

Table 3: Results of Drop Weight Test in Tabular Format (contd.)

Code	Tech[1].	Imp[2]. Dur. (ms)	Time Peak Acc. (ms)	Peak Acc. (g)	Peak Force Trans. (N)	Ips[3]. Peak Acc. (N.sec)	Ips. of Dur. (N.sec)	Disp. Peak Acc. (mm)	Disp. Imp. Dur. (mm)	Acc. Peaks	Force Peaks	Ht[4]. (cm)
t_2-5*	RCB	9	1.7	32.1	259	1.18	7.20	4.79	15.42	1	1	43.01
t_2-5	RCB	5.7	2	31	1335	0.99	2.82	5.60	13.94	1	1	42.92
t_2-6	RCB	7.5	1.7	52.9	2039	1.47	6.25	4.79	13.36	1	1	42.87
t_2-7	RCB	5	2.7	37	1637	1.01	1.53	7.83	13.49	1	1	43.24
t_2-8	RCB	8.5	1.2	39.5	1419	0.83	4.94	3.50	16.52	2	1	42.96
t_2-9	RCB	7	1.7	33.3	1038	0.70	3.61	5.01	16.16	1	1	43.41
Mean		6.7	1.9	38.7	1494	1.00	3.83	5.35	14.69			43.08
St. Dev.		1.4	0.6	8.6	373	0.29	1.83	1.59	1.52			0.23
t_2-10*	ABG	9.75	3	101	897	3.93	9.70	9.08	11.17	1	1	42.76
t_2-11*	ABG	12.7	2.7	80.6	3385	3.36	11.01	7.12	8.98	1	1	42.79
t_2-10	ABG	4.75	2.25	98	3808	2.62	4.96	7.42	11.42	1	1	43.10
t_2-11	ABG	12.5	3	88.9	4078	4.25	11.04	7.56	7.62	1	1	43.30
t_2-12	ABG	4.5	2.5	82	2699	3.71	3.59	5.35	8.59	1	1	43.21
t_2-13	ABG	4.2	2	68.9	2563	1.51	2.30	5.59	11.78	1	1	43.11
t_2-14	ABG	4.5	3.2	119.9	4563	5.33	6.39	8.07	9.38	1	1	43.37
Mean		6.1	2.6	91.5	3542	3.48	5.66	6.80	9.76			43.22
St. Dev.		3.6	0.5	19.1	876	1.47	3.38	1.24	1.80			0.12
t_2-15*	Intact	10	2.5	56.4	2946	2.91	6.63	6.32	15.12	2	1	42.88
t_2-15	Intact	12.25	2.5	102	4295	2.88	9.04	6.65	11.23	1	1	42.97
t_2-16	Intact	3.75	1.75	62.2	2523	1.53	2.22	5.52	10.09	1	1	42.71
t_2-17	Intact	3.75	1.5	67.2	2445	1.37	2.75	4.25	9.23	1	1	43.44
t_2-18	Intact	14	3	86.3	3899	4.45	11.33	7.33	5.17	1	1	43.11
Mean		8.4	2.2	79.4	3291	2.56	6.34	5.94	8.93			43.06
St. Dev.		5.5	0.7	18.3	946	1.43	4.55	1.35	2.64			0.30

Tech[1]: Technique.
Imp[2] : Impact.
Ips[3] : Impulse.
Ht[4] : Height
* : Tests were conducted again to obtain desired output.

Table 3: Results of Drop Weight Test in Tabular Format (contd.)

Code	Specimen	Comments
t_0-1	BO 5224	Cement broke. Mesh did not break
t_0-2	9905	Complete fracture
t_0-3	24	Complete fracture
t_0-4	9926	Complete fracture
t_0-5	44	Complete fracture
t_0-6	43	Specimen Broke
t_0-7	BO 5224	Fractured. Initially mass fell inadvertently.
t_0-8	9905	NO effect
t_0-9	9926	NO effect
t_0-10	24	NO effect
t_0-11	44	Specimen Broke
t_1-1	BO 5281	Specimen Broke
t_1-2	BO 5300	Complete fracture
t_1-3	BO 5286	Cement broke. Mesh did not break
t_1-4	BO 5288	Complete fracture
t_1-5	BO 5284	Complete fracture
t_1-6	BO 5285	Complete fracture
t_1-7	BO 5288	NO effect
t_1-8	BO 5284	NO effect
t_1-9	BO 5300	Specimen Broke
t_1-10	BO 5285	Specimen Broke
t_1-11	BO 5286	Specimen Broke
t_2-1	9916	Complete Fracture
t_2-2	BO 5502	Complete Fracture
t_2-3	9913	Complete Fracture
t_2-4	9912	Complete Fracture
t_2-5	295	Complete Fracture
t_2-6	5295	Complete Fracture
t_2-7	9911	Specimen Broke
t_2-8	9910	Complete Fracture
t_2-9	9907	Complete Fracture
t_2-10	9913	Complete Fracture
t_2-11	9907	No Effect
t_2-12	BO 5502	Specimen Broke
t_2-13	9912	Specimen Broke
t_2-14	9910	Complete Fracture
t_2-15	9916	No Effect
t_2-16	9906	Specimen Broke
t_2-17	295	Complete Fracture
t_2-18	5295	No Effect

4.3 Parameters Considered for Statistical Analysis

Parameters which were compared for observing the variations between the reconstruction techniques and their follow-up period were peak acceleration, peak force transmission, and time to peak acceleration. The remaining parameters related to impulse, displacement, and impact duration were not considered. These parameters, obtained by using mathematical formulas as explained in the data analysis section 3.6.5, form the output data sets of the time, acceleration, and force readings. The values of displacement to peak acceleration, displacement to impact duration, impulse to peak acceleration, and impulse during duration as described in data analysis section 3.6.5 may contain inconsistencies, which could have occurred due to indenter sliding, double impact, or complete fracture of the skull.

The parameters peak acceleration, peak force transmission, and time to peak acceleration were directly obtained from the drop weight test output. Statistical analysis was performed using MANOVA and Dunnetts test as explained in section 3.6.6.

4.4 Conclusion

Statistical analysis showed autogenous bone graft (ABG) as a better reconstruct when compared to reconstruction A (RCA, slow setting CCPP cement with titanium mesh scaffold) and Reconstruction B (RCB, fast setting CCPP cement with titanium mesh scaffold). ABG shows biostructural characteristics similar to Intact bone at t_2 period. RCB is a stiffer material when compared to RCA.

At t_0 period, all the reconstructions show no significant difference in biomechanical properties for peak acceleration, peak force transmission, and time to peak acceleration. Significant difference for peak acceleration ($p=0.0135$) and peak force

transmission (p=0.0204) is shown between ABG and RCA at t_1 period, showing results that RCA biomechanical properties decrease over a period of time. Peak acceleration and peak force transmission showed significant difference for ABG at t_2 period with all the rest of the groups. The high peak acceleration of ABG (91.5±19.1g) and peak force transmission (3542±876N) for ABG indicated that its biomechanical properties increased over time and was a better reconstruction technique than RCA and RCB. Time to peak acceleration showed no significant differences between RCA, RCB, and ABG when compared with a fixed follow-up period of either t_0, t_1, or t_2. However, it showed significant differences over a period of time, with t_0 being significantly different from t_1 and t_2 (p=0.0532). Dunnetts test at t_2 showed no significant differences between ABG and Intact bone for peak acceleration and peak force transmission. However, significant differences were observed between RCA and Intact bone ($p<0.0001$) and RCB and Intact bone ($p<0.0001$). Hence, ABG biostructural characteristics are similar to Intact bone at t_2. Significant differences were not obtained to differentiate between RCA and RCB. However, data analysis shows that peak acceleration and peak force transmission for RCA decreases, whereas displacement to peak acceleration increases over a period of time. Moreover, no significant differences could be obtained for peak acceleration and peak force transmission between RCB and ABG at t_1, unlike RCA and ABG at t_1. Hence, RCB shows to be a stiffer reconstruction structure compared to RCA.

4.5 Power of the Test

Sample size determination was not a part of this author's study. This author was approached after Stage A was completed in 2004. Stage A consisted of reconstructing the sheep skulls based on their follow-up period. This author was asked to complete Stage B,

experimental testing and data analysis of the reconstructions. Stage C consisting of histological analysis was completed by The Cleveland Clinic Foundation, Cleveland, OH.

Power of the test was found after experimental testing was determined by the method described by Sokal et al. [35]. The power of the test was found to be 95%.

CHAPTER V

DISCUSSION

5.1. Justification for the Testing Apparatus Selection

Motorcycle helmets require mandatory approval following FMVSS218 standard from the Department of Transportation (DOT) of the United States. Snell Memorial Foundation evaluates protective headgear for motorized and non-motorized sports. Drop weight tests used to measure peak acceleration provide the data to evaluate the impact resistance of the helmets [10,34,37]. Headgear is an external cranial cover and the protocol developed to test an integral cranial cover was similar.

The study compared the biomechanical properties of two reconstruction structures (slow setting and fast setting carbonated calcium phosphate cements with titanium mesh scaffolds) with autogenous bone grafts on full-thickness reconstructions of cranial bone defects. Biostructural characteristics were compared between intact bone (control group) and three reconstruction structures during a follow-up period t_2 (12 months).

Compressive strengths of hydroxyapatite (HA) cements have been reported in the range from 10 to 80Mpa, compared to bone with a range of 300 to 400Mpa [23,26]. HA cements are brittle with an average tensile strength reported to be 15Mpa. Previous studies have been based on evaluating the compressive strengths of (HA) cements [9,18,23,26]. The cranium typically fails through linear fractures due to tensile forces at the site of impact at a trauma rate in the range of 5 to 40 milliseconds.

Common impact injuries would be falls and vehicular accidents that occur at approximately 8 milliseconds. To study HA cements in relation to cranial defect reconstruction, the cement must not only be exposed to compressive but tensile and torsional forces as well [10,23,26,28,41,43].

Titanium mesh used in full thickness defects with HA cement provides only a containment method to control setting of the cement. The mesh tends to buckle and bend under applied force exposing the HA cement to further tensile forces, propagating fracture of the cement. According to reports the mesh does not improve impact resistance of the reconstruction [10,23,26]. In this study, carbonated calcium phosphate (CCPP) cement with titanium mesh was not evaluated separately, but considered as a reconstruct. Titanium mesh does not have viscoelastic properties. However, the bone and connective tissue interface with titanium mesh functions as a viscoelastic material [22,23,27,48].

Bone is a viscoelastic material and hence the cortical and trabecular bone mechanical properties vary with strain rate. Under high strain rate, bone fractures at higher ultimate strength but lower strain. Cranial bone mechanical properties have been reported to be rate sensitive in tension. The effect of chemical composition, setting time since mixing, temperature, hydration, particle size, and porosity affect the viscoelastic behavior of HA cement [2,12,19,22,38,48].

HA cement studies reporting the strength and stiffness have been performed using push out and indentation tests [9,18,26]. However, servo-hydraulic machines cannot reproduce high strain rates for impact evaluation of the HA cement. Low velocity impacts resulting from minor trauma due to a fall or altercation have been studied using cadaver heads at zero time by drop weight test. Force of 1200N was reported to induce

predictable fractures in full thickness skull defects reconstructed with Norian® cement and titanium mesh [23]. This study verifies the peak force transmission values for reconstruction structures RCA, RCB, and ABG at zero time 904±265N, 702±348N, and 928±321N, respectively. However, in this study, the peak acceleration parameter is considered due to factors mentioned above, considering that peak force transmission values could have been affected due to indenter sliding, double bounce, and jig specification.

Healing at the defect site mainly occurs through osteonal remodeling across the fracture line, a process known as primary fracture healing. Basic multicellular units consisting of osteoclasts and osteoblasts tunnel through the compact bone [22]. Considering real life injury situations of cranial defects reconstructions with HA cement, the interface of bone transition area and HA cement with titanium mesh structure should also be considered during experimental testing. Impact evaluation using a drop weight test to determine the biomechanical properties of the cranial defect reconstruction is the correct method to measure the impact resistance of the structure.

5.2 Events During Tests Resulting in Modification of the Testing Protocol

During a test on the left side of specimen t_0 period (animal code BO 5224, group 3.1.a.), the mass fell inadvertently while preparing the test setup displacing ABG (Figure 5.1). The ABG was aligned as before. The right side of the specimen was tested as per the protocol and the readings for the right side were not affected since it was tested before. 4 point support was used.

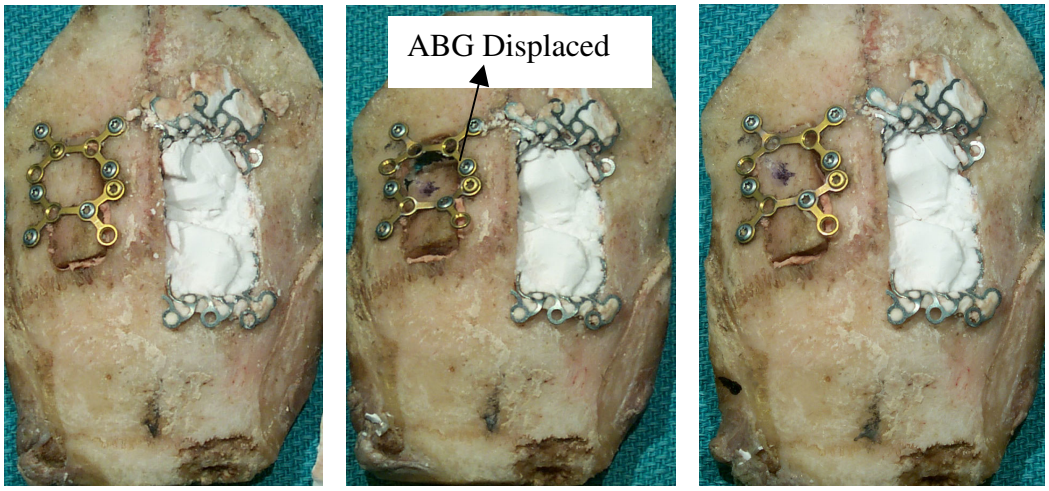

Figure 5.1. Error occurred during test as mass fell advertently.

During a test of specimen t_0 period (animal code 43, group 3.1.b), the right side test fractured the specimen (Figure 5.2). The left side of the specimen, therefore, could not be tested. Data for the right side were collected as per test protocol. Similar instances where the specimen broke are given in Table 3.

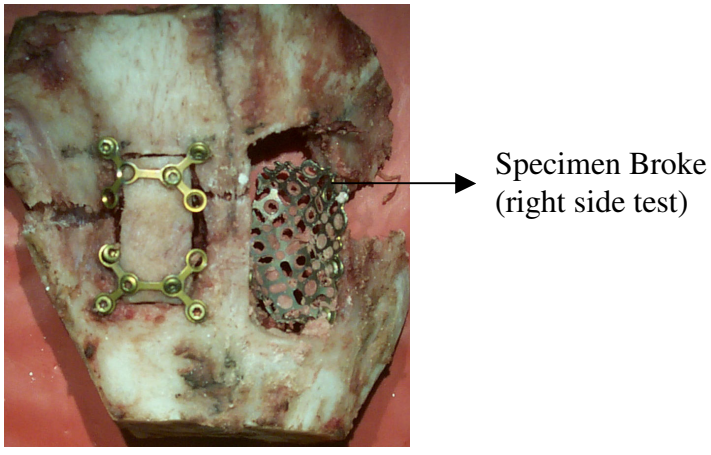

Figure 5.2. Specimen broke during experimental testing.

The initial height (measured between the tip of the indenter and the skull) for the test carried out for t_0 period was approximately 19cm (Table 3). While testing for specimen t_1 period (animal code BO 5288, group 1B), right side testing did not produce the impact force required (the skull did not fracture upon test). To avoid multiple impacts and to ensure that the skulls fracture in a single test, the height between the indenter and skull was increased to approximately 42cm (Figure 5.3). As mentioned previously, actual impact height was always determined from integration of the accelerometer readings.

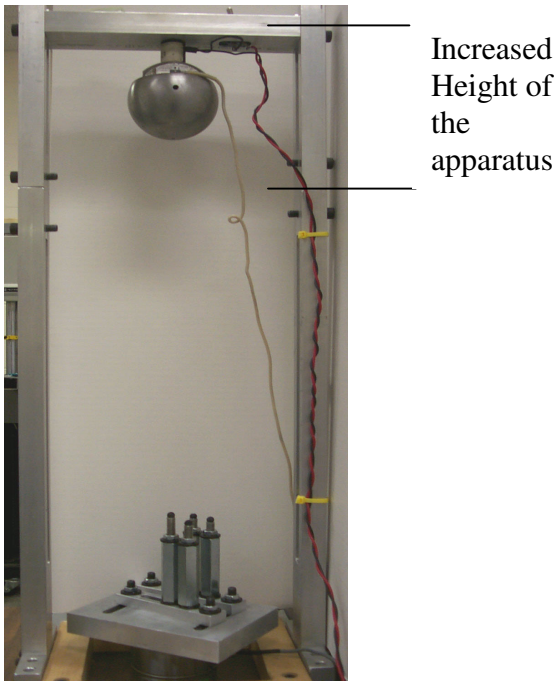

Figure 5.3. Increase in height of the testing apparatus between tests.

For specimen t_1 period (animal code BO 5288, group 1B), the periosteum was removed from the outer surface of the specimen by Dr.Andrea Moreira-Gonzalez and Dr.Glen Njus (Figure 5.4). This was done because the indenter seemed to be sliding and actual force was not transmitted over a particular point, in a normal orientation with

respect to the surface as tangent. The surface procedure increased the coefficient of friction.

Actual specimen

Cleaning and smoothing the periosteum surface

Figure 5.4. Cleaning of the periosteum of a specimen during test.

To increase the coefficient of friction and help prevent the indenter from sliding upon impact on the specimen, 120 fine grain sandpaper with an adhesive back was attached at the base of the indenter to replace the skin resembling surface. Sandpaper was used only once during testing at t_1 period (animal code BO 5288, group 1B). However, these values were not considered during statistical analysis since the specimen did not fracture. The specimen was re-tested.

During initial tests, the indenter appeared to be bent upon impact. The length of the indenter was modified from 3.17 cm to 2.54 cm before testing specimen t_1 period (animal code BO 5288, group 1B). This modified indenter was used for the remaining tests (Figure 5.5). The weight of the changed indenter was measured and incorporated in the data analysis.

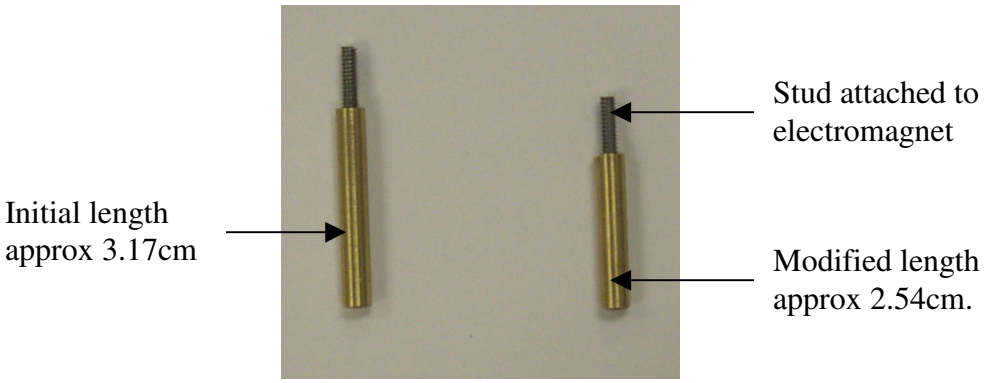

Figure 5.5. Modifications made to the indenter.

The indenter was further modified to prevent sliding and provide a relatively stable impact during testing at t_2 period involving all RCB and ABG reconstructs as shown in Figure 5.6. The change in indenter gave a relatively stable impact, which was evident from the high peak acceleration calculated for RCB and ABG.

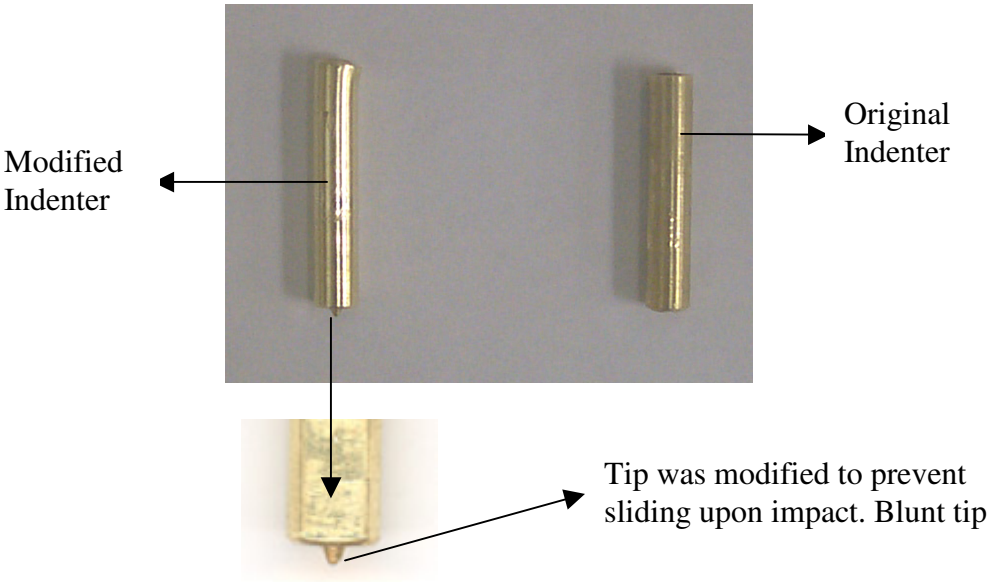

Figure 5.6. Modifications made to the indenter tip.

During t_1 period (animal code BO 5288, group 1B) test, scotch tape and rubber bands were used to keep the specimen intact (Figure 5.7). No skin resembling surface was used (FDA-Buna Nitrile Rubber could be the cause of slippage during impact). The scotch tape and rubber bands were used in other trials, depending upon the condition of the specimen.

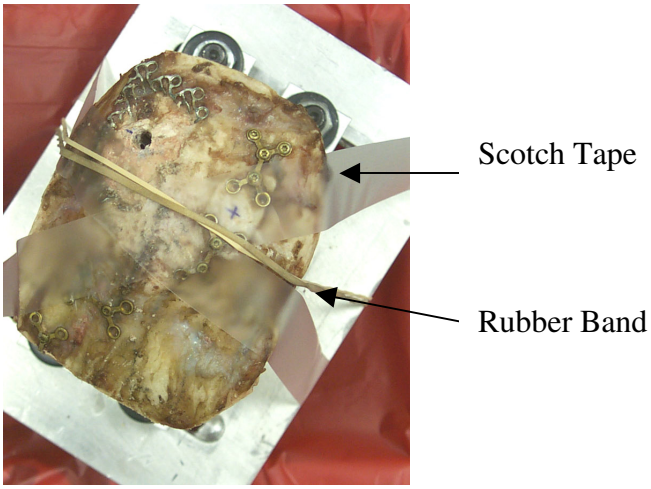

Figure 5.7. Extra support used for stabilization of the specimen.

5.3 Limitations of the Study

1. The reconstructions were carried out such that RCA or RCB were always on the right side of the specimen. The ABG reconstruction and intact bone were always on the left side. According to biometry principles, random assignment of the reconstructions should be conducted to avoid any dependent effect on the sides of the specimen.

2. The jig used for testing was designed taking into account factors such as cost, time, and repeatability. The specimen could be supported on a different base to avoid use of adhesive tapes and rubber bands. A negative of alginate (dental impression) material could be made to mold the shape of the base of sheep skull. A positive of

polymethylmethacrylate (PMMA) from the negative could be made to replicate the outer base of the skull on which the specimen could be rested.

3. A uniaxial accelerometer was used for measuring peak acceleration only in the vertical direction. A triaxial accelerometer could be used to measure peak acceleration in all orientations (x,y, and z) thus providing true spatial orientation of the mass prior to and during impact, which were masked by the use of uniaxial accelerometer.

4. The peak acceleration and peak force transmission values measured for the reconstructions in this study may have differed partially due to variations in the jig, indenter, and specimen orientation.

5.4 Future Work on the Study

1. Analytical analysis with a finite element analysis (FEA) package using LS-Dyna (PC-DYNA_970, Livermore Software Technology Corporation, Livermore, CA) or any other software could be done to study the dynamic behavior of the drop weight test on the sheep skull.

2. Since autogenous bone graft was found to be a better reconstruction technique, a new synthetic technique could be developed replacing the existing techniques.

BIBLIOGRAPHY

1. Burstein, F., S. Cohen, R. Hudgins, W. Boydston, and C. Simms, 1999. The use of hydroxyapatite cement in secondary craniofacial reconstruction. Plastic and Reconstructive Surgery 104, 1270-1275.

2. Cho, Y., and A. Gosain, 2004. Biomaterials in craniofacial reconstruction. Clinics in Plastic Surgery 31, 377-385.

3. Clokie, C., M. Hassan, M. Jackson, and G. Sandor, 2002. Closure of critical sized defects with allogenic and alloplastic bone substitutes. J. Craniofacial Surgery13, 111-121.

4. Costantino, P., C. Friedman, K. Jones, L. Chow, H. Pelzer, and G. Sisson, 1991. Hydroxyapatite cement: I. Basic chemistry and histologic properties. Archives of Otolaryngology-Head and Neck Surgery 117, 379-384.

5. Costantino, P., J. Chaplin, M. Wolpoe, P. Catalano, C. Sen, J. Bederson, and S. Govindaraj, 2000. Applications of fast setting hydroxyapatite cement. Otolaryngology-Head and Neck Surgery 123, 409-412.

6. Costantino, P., C. Friedman, K. Jones, L. Chow, and G. Sisson, 1992. Experimental hydroxyapatite cement cranioplasty. Plastic and Reconstructive Surgery 90, 174-187.

7. Ducic, Y., 2002. Titanium mesh and hydroxyapatite cement cranioplasty: a report of 20 cases. J. Oral Maxillofacial Surgery 60, 272-276.

8. Durham, S., J. McComb, and M. Levy, 2003. Correction of large (>25 cm^2) cranial defects with "reinforced" hydroxyapatite cement: technique and complications. Neurosurgery 52, 842-845.

9. Elshahat, A., M. Shermak, N. Inoue, E. Chao, and P. Manson, 2004. The use of novabone and norian in cranioplasty: a comparative study. J. Craniofacial Surgery 15, 483-489.

10. Eppley, B., 2005. Invited discussion: A comparison of resistance to fracture among four commercially available forms of hydroxyapatite cement. Annals of Plastic Surgery 55, 93.

11. Eppley, B., L. Hollier, and S. Stal, 2003. Hydroxyapatite cranioplasty: 2. Clinical experience with a new quick-setting material. J. Craniofacial Surgery 14, 209-214.

12. Fernandez, E. M. Ginebra, M. Boltong, F. Driessens, J. Ginebra, E. De Maeyer, R. Verbeeck, and J. Planell, 1996. Kinetic study of the setting reaction of a calcium phosphate bone cement. J. Biomedical Materials Research 32, 367-374.

13. Gosain, A., and the Plastic Surgery Education Foundation Data Committee, 2005. Biomaterials for reconstruction of the cranial vault. Plastic and Reconstructive Surgery 116, 663-666.

14. Gosain, A., L. Song, P. Riordan, M. Amarante, P. Nagy, C. Wilson, J. Toth, and J. Ricci, 2002. A 1-year study of osteoinduction in hydroxyapatite-derived biomaterials in an adult sheep model, Part I. Plastic and Reconstructive Surgery 109, 619-630.

15. Gosain, A., L. Song, P. Riordan, M. Amarante, P. Nagy, C. Wilson, J. Toth, and J. Ricci, 2004. A 1-year study of osteoinduction in hydroxyapatite-derived biomaterials in an adult sheep model, Part II. Bioengineering implants to optimize bone replacement in reconstruction of cranial defects: Plastic and Reconstructive Surgery114, 1155-1163.

16. Greenberg, B. and S. Schneider, 2005. Alloplastic reconstruction of large cranio-orbital defects: a comparative evaluation. Annals of Plastic Surgery 55, 43-51.

17. Havlik, R., and the PSEF Data Committee, 2002. Hydroxyapatite. Plastic and Reconstructive Surgery 110, 1176-1179.

18. Ichiro, O., T. Tohru, N. Takehiko, and O. Tetsuro, 1998. Determinations of strength of synthetic hydroxyapatite ceramic implants. Plastic and Reconstructive Surgery 102, 807-813.

19. Lee, A., R. Ling, S. Gheduzzi, J. Simon, and R. Renfro, 2002. Factors affecting the mechanical and viscoelastic properties of acrylic bone cement. J. Material Science: Materials in Medicine 13, 723-733.

20. Losee, J., J. Karmacharya, F. Gannon, A. Slemp, G. Ong, O. Hunenko, A. Gorden, S. Bartlett, and R. Kirschner, 2003. Reconstruction of the immature craniofacial skeleton with a carbonated calcium phosphate bone cement: Interaction with bioresorbable mesh. J. Craniofacial Surgery 14, 117-124.

21. Magee, W., N. Ajkay, N. Freda, and R. Rosenblum, 2004. Use of fast setting hydroxyapatite cement for secondary craniofacial contouring. Plastic and Reconstructive Surgery 114, 289-297.

22. Martin, R., D. Burr, and N. Sharkey. Skeletal Tissue Mechanics. © 1998 Springer-Verlag New York, Inc. 392pp.

23. Matic, D., and P. Manson, 2004. Biomechanical analysis of hydroxyapatite cement cranioplasty. J. Craniofacial Surgery 15, 415-423.

24. Matic, D. and J. Phillips, 2002. A contraindication for the use of hydroxyapatite cement in the pediatric population. Plastic and Reconstructive Surgery110, 1-5.

25. Mathur, K., S. Tatum, and R. Kellman, 2003. Carbonated apatite and hydroxyapatite in craniofacial reconstruction. Archives of Facial Plastic Surgery 5, 379-383.

26. Miller, L., A. Guerra, R. Bidros, C. Trahan, R. Baratta, and S. Metzinger, 2005. A comparison of resistance to fracture among four commercially available forms of hydroxyapatite cement. Annals of Plastic Surgery 55, 87-92.

27. Moreira-Gonzalez, A., I.Jackson, T. Miyawaki, K. Barakat, and V. DiNick, 2003. Clinical outcome in cranioplasty: critical review in long-term follow-up. J. Cranofacial Surgery 14, 144-153.

28. Moreira-Gonzalez, A., T. Baurer, A. Parikh, M. Siemionow, and J.Zins, 2006. Biomechanical analysis of long-term reconstruction of full thickness skull defects using hydroxyapatite cement (Norian CRS and Fast Set Putty) in a sheep model. 51st Annual Meeting of the Plastic Surgery Research Council, Dana Point, CA., USA.

29. Rohlf, F., and R. Sokal. Statistical Tables, 3rd edition. © 1995 W. H. Freeman and Co.: New York. 199 pp.

30. Ruiz, R., T. Turvey, B. Costello, T. Tejera, and J. Tinerfe, 2005. Cranial bone grafts: craniomaxillofacial applications and harvesting techniques. Atlas of the Oral and Maxillofacial Surgery Clinics of North America 13, 127-137.

31. Schmitz, J., J. Hollinger, and S. Milam, 1999. Reconstruction of bone using calcium phosphate bone cements: a critical review. J. Oral and Maxillofacial Surgery 57, 1122-1126.

32. Scott, M., H. Wycis, and F. Murtagh, 1962. Long term evaluation of stainless steel cranioplasty. Surgery, Gynecology and Obstetrics 115, 453-461.

33. Smart, J., J. Karmacharya, F. Gannon, G. Ong, O. Jackson, S. Bartlett, R. Poser, and R. Kirschner, 2005. Repair of the immature and mature craniofacial skeleton. Plastic and Reconstructive Surgery 15, 1642-1650.

34. Snell Memorial Foundation, Inc., 2005. Standard for protective headgear for use with motorcycle and other motorized vehicles. North Highlands, CA., USA.

35. Sokal, R., and F. Rohlf. Biometry: the principles and practice of statistics in biological research. 3rd edition. © 1995 W. H. Freeman and Co.: New York. 887 pp.

36. Stal, S., K. Tjelmeland, J. Hicks, N. Bhatia, B. Eppley, and L. Hollier, 2001. Compartmentalized bone regeneration of cranial defects with biodegradable barriers: an animal model. J. Craniofacial Surgery 12, 41-47.

37. U.S. Department of Transportation (DOT), 2001. Federal Motor Vehicle Safety Standard 218 (FMVSS 218) 49, 643-659.

38. Verdonschot, N., C. van Hal, B. Schreurs, P. Buma, R. Huiskes, and T. Slooff, 2001. Time-dependent mechanical properties of HA/TCP particles in relation to morsellized bone grafts for use in impaction grafting. J. Biomedical Materials Research 58, 599-604.

39. Verret, D., D. Yadranko, L. Oxford, and J. Smith, 2005. Hydroxyapatite cement in craniofacial reconstruction. Otolaryngology-Head and Neck Surgery 133, 897-899.

40. Wolfe, S., 1982. Autogenous bone grafts versus alloplastic material in maxillofacial surgery. Clinics in Plastic Surgery 9, 539-540.

41. Wood, J., 1971. Dynamic response of human cranial bone. J. Biomechanics 4, 1-12.

42. Woodhall, B. and G. Spurling, 1945. Tantalum cranioplasty for war wounds of the skull. Annals of Surgery 121, 649-671.

43. Yoganandan, N., and F. Pintar, 2004. Biomechanics of temporo-parietal skull fracture. Clinical Biomechanics 19, 225-239.

44. http://face-and-emotion.com/dataface/physiognomy/cranium.jsp; online link. [dated January 15, 2006].

45. http://www.ivy-rose.co.uk/Topics/Bones_CranialandFacial.htm; online link [dated January 15, 2006].

46. http://www.synthes.com/html/Norian_Craniofacial.4327.0.html; online link [dated January 15, 2006].

47. https://www2.carolina.com/webapp/wcs/stores/servlet/CarolinaBio/images/medium/246301_ske.jpg; online link [dated: January, 15 2006].

48. http://ttb.eng.wayne.edu/~grimm/BME5370/Lect3Out.html#ViscoelasticProps; online link [dated: July 12, 2006]

49. http://www.skullsite.co.uk/Human/human_lat.jpg; online link [dated: November 12, 2006]

APPENDICES

APPENDIX A

CLASSIFICATION OF SAMPLES GIVEN FOR TEST

Table 4. Information on classification of samples based on their follow-up period given for test

Follow-up period	Reconstruction Technique	Groups	Animal Number	Animal Code
t_0 (0 month)	RCA (r) ABG (l)	3.1.a	19	24
			20	BO 5224
			21	9905
	RCB (r) ABG (l)	3.1.b	16	44
			17	9926
			18	43
t_1 (6 month)	RCA (r) ABG (l)	1A	27	BO 5281
			26	BO 5286
			25	BO 5300
	RCB (r) ABG (l)	1B	23	BO 5284
			22	BO 5288
			24	BO 5285
t_2 (12 month)	RCA (r) ABG (l)	1A	13	9912
			14	9913
			15	BO 5502
	RCB (r) ABG (l)	1B	10	9907
			11	9910
			12	9911
	RCA (r) Intact (l)	2A	7	9906
			8	9923
			9	9916
	RCB (r) Intact (l)	2B	4	295
			5	9919
			6	5295

APPENDIX B

SPECIFICATIONS USED FOR DROP WEIGHT TEST

1. Mass: Spherical mass of 3.222 kg (excluding weight of indenter) was attached to the electromagnet.

2. Accelerometer: A piezoresistive accelerometer with a 2000 g range was used. (Endevco piezoresistive accelerometer – Model 2264-2000, CA).

3. Load Cell: A 2000 lb stainless steel load cell was used (Lebow – Model 3169-2000, Eatron Corporation, Troy, Michigan).

4. Indenter: A brass rod was used with a stud attachment. Modifications were made in the length and the tip of the indenter in between tests.

5. Skin resemblance surface: FDA-Buna Nitrile Rubber – Hardness 60 D; Thickness 1.6 mm; Elastic Modulus 3 MPa. This rubber was attached to the base of indenter for initial tests to resemble a skin surface. Due to slippage of the indenter it was later removed.

6. Neoprene Rubber Balls: The specimen was supported on neoprene rubber balls of diameter 0.95 cm.

7. Sand paper: 120 fine grain sand paper with adhesive back.

APPENDIX C

PICTURES OF A SPECIMEN SHOWING THE RESULTS OF A DROP WEIGHT TEST

Specimen at t_0 (animal code 44, group 3.1.b); right side - RCB, left side - ABG.

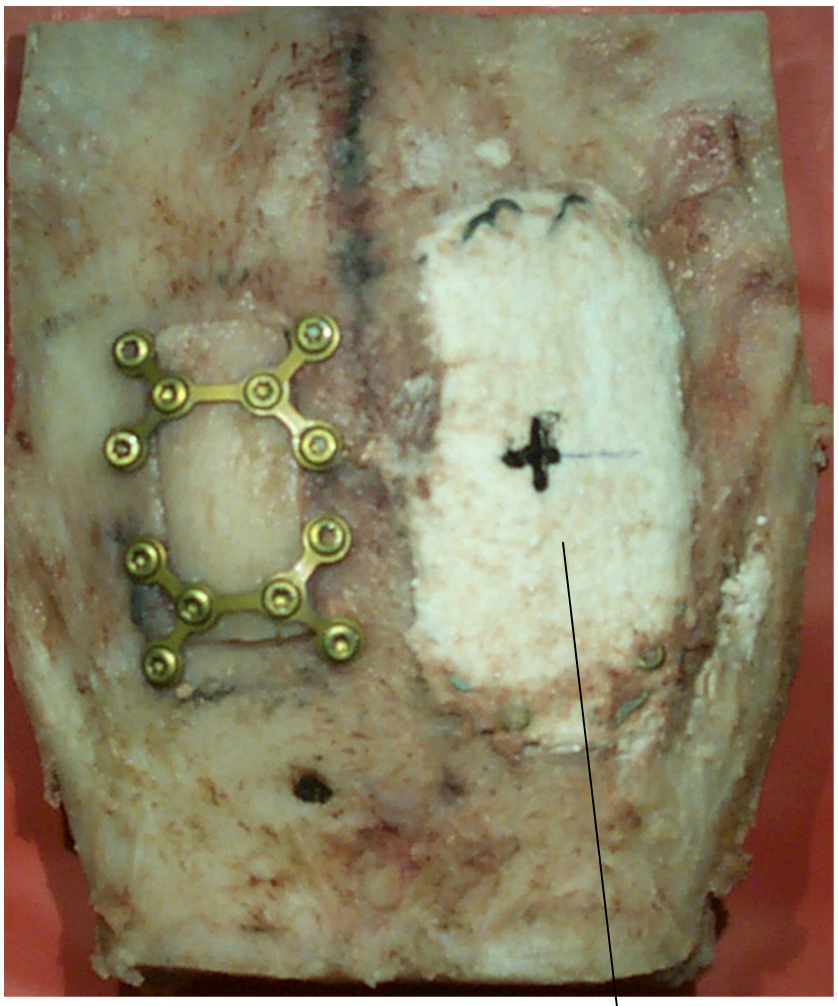

Figure C.1. Top view of specimen marked and ready to be experimentally test.

Figure C.2. Bottom view of specimen marked and ready to be experimentally test.

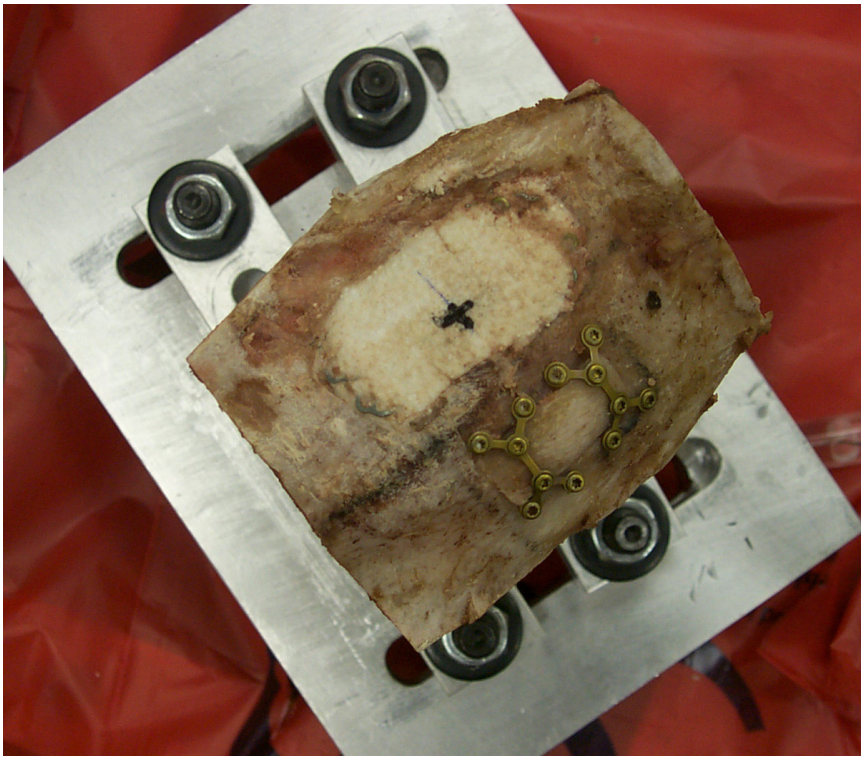

Figure C.3. Specimen placed on jig and right side ready for impact.

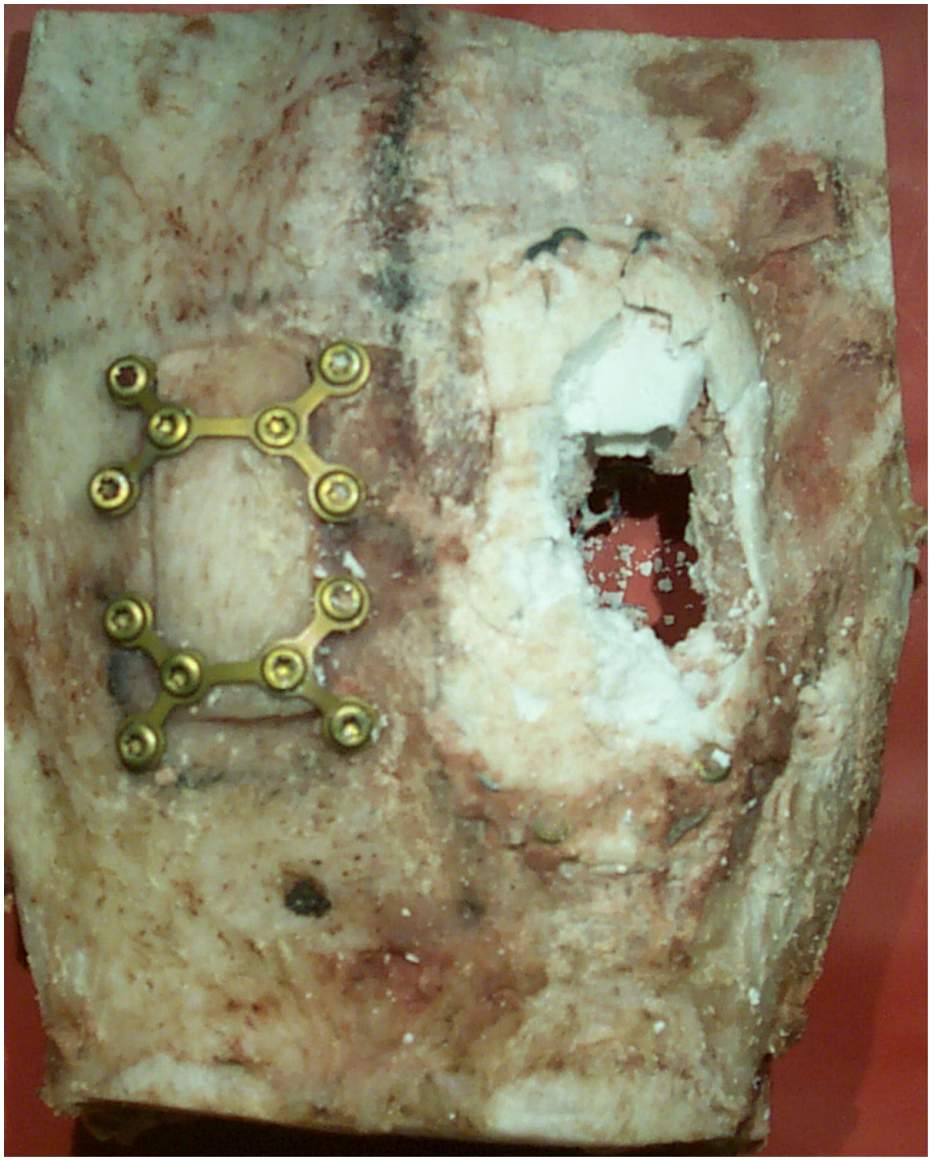

Figure C.4. Top view of specimen after impact upon RCB reconstruct (right side).

Figure C.5. Top view of specimen showing results after impact on ABG (left side). The specimen completely broke.

APPENDIX D

JIG SPECIFICATIONS

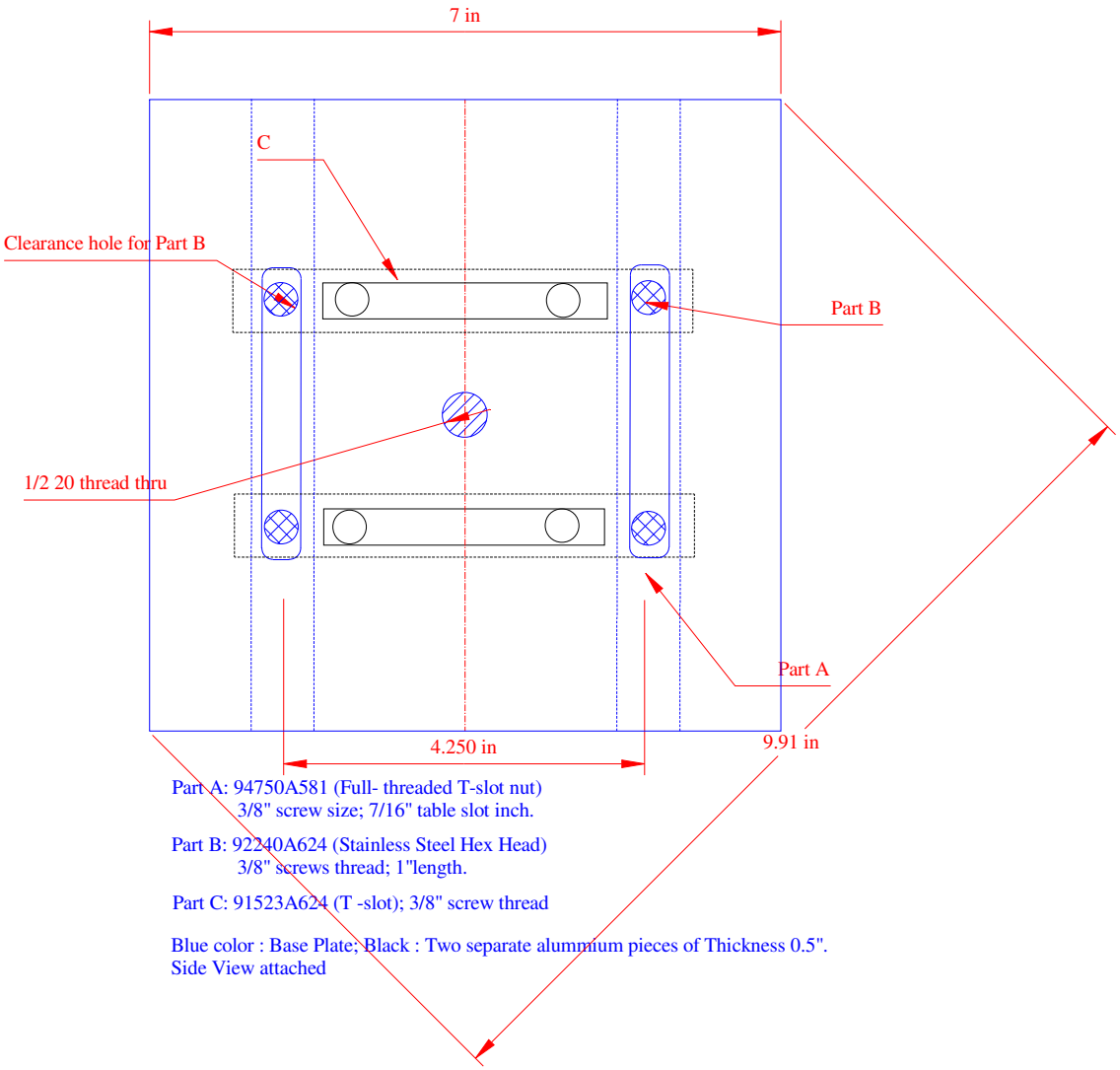

Figure D.1. Jig Specification

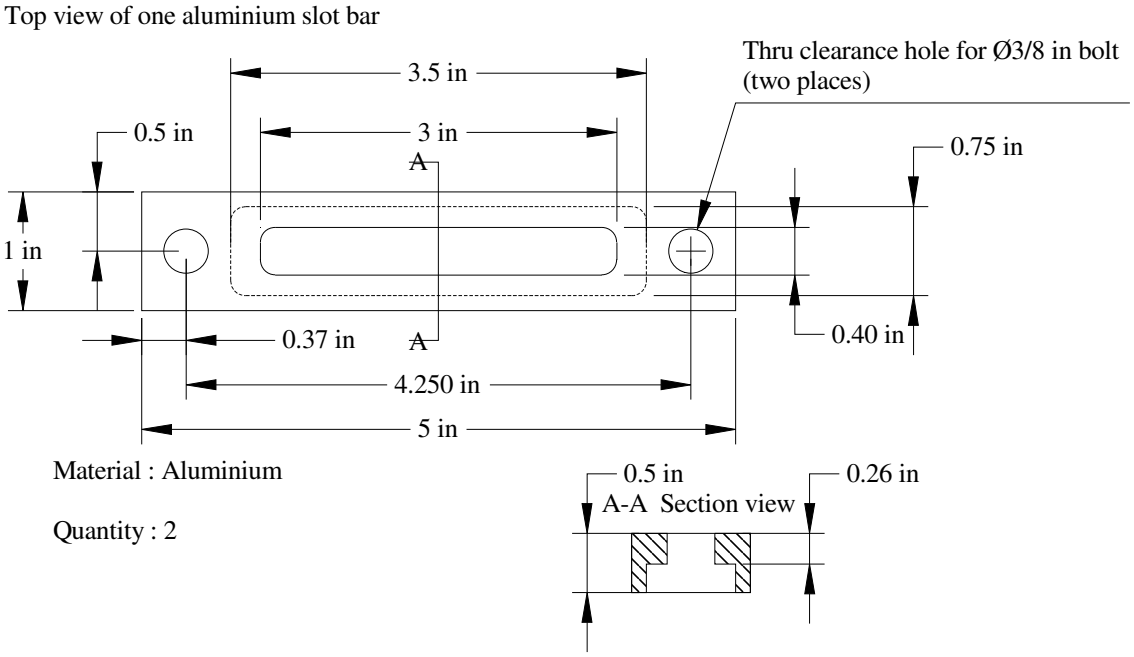

Figure D.1. Jig Specification (contd…)

APPENDIX E

STATISTICAL RESULTS IN SAS

```
*/Case1: MANOVA /;
data;
input material $ month $ n @;
do trial=1 to n;
input force acceleration time @@;
output;
end;
cards;
RCA 0 3 599 23.8 2.3 1065 31.3 3.5 1049 32.0 2.5
RCB 0 3 1070 26.4 3.2 657 16.0 2.2 378 11.5 2.7
ABG 0 5 833 23.9 2.2 458 16.1 3.5 1264 34.2 6.0 897 34.2 4.0 1188 34.0 4.2
RCA 6 3 190 6.8 2.5 261 11.2 2.2 931 31.2 2.5
RCB 6 3 1975 60.8 1.7 846 23.7 2.2 799 24.1 3.2
ABG 6 5 1960 55.3 1.5 2444 55.6 2.7 1326 47.7 1.5 2368 75.0 2.7 1442 29.8 4.0
RCA 12 4 291 7 4.25 853 28.7 3.5 544 16.1 2 763 20.8 3.7
RCB 12 5 1335 31 2 2039 52.9 1.7 1637 37 2.7 1419 39.5 1.2 1038 33.3 1.7
ABG 12 5 2699 82 2.5 2563 68.9 2 3808 98 2.25 4563 119.9 3.2 4078 88.9 3
;
proc print;
run;
proc glm;
class material month;
model force acceleration time = material | month;
lsmeans material*month/pdiff= all;
means material/SNK;
means month/SNK;
run;
```

The GLM Procedure

Class Level Information

Class	Levels	Values
material	3	ABG RCA RCB
month	3	0 12 6

Number of observations 36

The GLM Procedure

Dependent Variable: force

Source	DF	Sum of Squares	Mean Square	F Value	Pr > F
Model	8	32789413.58	4098676.70	16.07	<.0001
Error	27	6886649.42	255061.09		
Corrected Total	35	39676063.00			

R-Square	Coeff Var	Root MSE	force Mean
0.826428	35.21458	505.0357	1434.167

Source	DF	Type I SS	Mean Square	F Value	Pr > F
material	2	13864583.12	6932291.56	27.18	<.0001
month	2	9483842.62	4741921.31	18.59	<.0001
material*month	4	9440987.84	2360246.96	9.25	<.0001

Source	DF	Type III SS	Mean Square	F Value	Pr > F
material	2	14009031.39	7004515.69	27.46	<.0001
month	2	6836275.56	3418137.78	13.40	<.0001
material*month	4	9440987.84	2360246.96	9.25	<.0001

The GLM Procedure

Dependent Variable: acceleration

Source	DF	Sum of Squares	Mean Square	F Value	Pr > F
Model	8	20194.74667	2524.34333	14.40	<.0001
Error	27	4733.24333	175.30531		
Corrected Total	35	24927.99000			

R-Square	Coeff Var	Root MSE	acceleration Mean
0.810123	33.36487	13.24029	39.68333

Source	DF	Type I SS	Mean Square	F Value	Pr > F
material	2	8915.531303	4457.765652	25.43	<.0001
month	2	5161.351362	2580.675681	14.72	<.0001
material*month	4	6117.864001	1529.466000	8.72	0.0001

Source	DF	Type III SS	Mean Square	F Value	Pr > F
material	2	8941.660970	4470.830485	25.50	<.0001
month	2	3622.917692	1811.458846	10.33	0.0005
material*month	4	6117.864001	1529.466000	8.72	0.0001

The GLM Procedure

Dependent Variable: time

Source	DF	Sum of Squares	Mean Square	F Value	Pr > F
Model	8	14.33229167	1.79153646	2.49	0.0362
Error	27	19.41020833	0.71889660		
Corrected Total	35	33.74250000			

R-Square	Coeff Var	Root MSE	time Mean
0.424755	30.92563	0.847878	2.741667

Source	DF	Type I SS	Mean Square	F Value	Pr > F
material	2	4.28009848	2.14004924	2.98	0.0679
month	2	4.71017975	2.35508987	3.28	0.0532
material*month	4	5.34201344	1.33550336	1.86	0.1470

Source	DF	Type III SS	Mean Square	F Value	Pr > F
material	2	3.16916632	1.58458316	2.20	0.1298
month	2	3.05569295	1.52784647	2.13	0.1389
material*month	4	5.34201344	1.33550336	1.86	0.1470

The GLM Procedure
Least Squares Means
Adjustment for Multiple Comparisons: Tukey-Kramer

material	month	force LSMEAN	LSMEAN Number
ABG	0	928.00000	1
ABG	12	3542.20000	2
ABG	6	1908.00000	3
RCA	0	904.33333	4
RCA	12	612.75000	5
RCA	6	460.66667	6
RCB	0	701.66667	7
RCB	12	1493.60000	8
RCB	6	1206.66667	9

Least Squares Means for effect material*month
Pr > |t| for H0: LSMean(i)=LSMean(j)

Dependent Variable: force

i/j	1	2	3	4	5	6	7	8	9
1		<.0001	0.0948	1.0000	0.9890	0.9324	0.9994	0.6996	0.9972
2	<.0001		0.0007	<.0001	<.0001	<.0001	<.0001	<.0001	<.0001
3	0.0948	0.0007		0.1872	0.0172	0.0135	0.0615	0.9235	0.6185
4	1.0000	<.0001	0.1872		0.9972	0.9730	0.9999	0.7978	0.9978
5	0.9890	<.0001	0.0172	0.9972		1.0000	1.0000	0.2326	0.8271
6	0.9324	<.0001	0.0135	0.9730	1.0000		0.9996	0.1614	0.6762
7	0.9994	<.0001	0.0615	0.9999	1.0000	0.9996		0.4649	0.9437
8	0.6996	<.0001	0.9235	0.7978	0.2326	0.1614	0.4649		0.9966
9	0.9972	<.0001	0.6185	0.9978	0.8271	0.6762	0.9437	0.9966	

material	month	acceleration LSMEAN	LSMEAN Number
ABG	0	28.4800000	1
ABG	12	91.5400000	2
ABG	6	52.6800000	3
RCA	0	29.0333333	4
RCA	12	18.1500000	5
RCA	6	16.4000000	6
RCB	0	17.9666667	7
RCB	12	38.7400000	8
RCB	6	36.2000000	9

The GLM Procedure
Least Squares Means
Adjustment for Multiple Comparisons: Tukey-Kramer

Least Squares Means for effect material*month
Pr > |t| for H0: LSMean(i)=LSMean(j)

Dependent Variable: acceleration

i/j	1	2	3	4	5	6	7	8	9
1		<.0001	0.1358	1.0000	0.9577	0.9373	0.9713	0.9435	0.9960
2	<.0001		0.0022	<.0001	<.0001	<.0001	<.0001	<.0001	0.0001
3	0.1358	0.0022		0.3011	0.0147	0.0204	0.0299	0.7615	0.7389
4	1.0000	<.0001	0.3011		0.9729	0.9565	0.9800	0.9822	0.9989
5	0.9577	<.0001	0.0147	0.9729		1.0000	1.0000	0.3664	0.6910
6	0.9373	<.0001	0.0204	0.9565	1.0000		1.0000	0.3707	0.6623
7	0.9713	<.0001	0.0299	0.9800	1.0000	1.0000		0.4641	0.7491
8	0.9435	<.0001	0.7615	0.9822	0.3664	0.3707	0.4641		1.0000
9	0.9960	0.0001	0.7389	0.9989	0.6910	0.6623	0.7491	1.0000	

The GLM Procedure

Student-Newman-Keuls Test for time

NOTE: This test controls the Type I experimentwise error rate under the complete null hypothesis but not under partial null hypotheses.

Alpha	0.05
Error Degrees of Freedom	27
Error Mean Square	0.718897
Harmonic Mean of Cell Sizes	11.84615

NOTE: Cell sizes are not equal.

Number of Means	2	3
Critical Range	0.7148293	0.8637921

Means with the same letter are not significantly different.

SNK Grouping	Mean	N	month
A	3.3000	11	0
B	2.5500	14	12
B			
B	2.4273	11	6

```
*/Case2: Dunnett's test/;
data;
input material $ n @;
do trial=1 to n;
input force acceleration time @@;
output;
end;
cards;
RCA 4 291 7 4.25 853 28.7 3.5 544 16.1 2 763 20.8 3.7
RCB 5 1335 31 2 2039 52.9 1.7 1637 37 2.7 1419 39.5 1.2 1038 33.3 1.7
ABG 5 2699 82 2.5 2563 68.9 2 3808 98 2.25 4563 119.9 3.2 4078 88.9 3
Intact 4 2523 62.2 1.75 4295 102 2.5 2445 67.2 1.5 3899 86.3 3
;
proc print;
run;
proc glm;
class material;
model force acceleration time = material;
means material/ dunnett ('Intact');
run;
```

The GLM Procedure

Class Level Information

Class	Levels	Values
material	4	ABG Intact RCA RCB

Number of observations 18

The GLM Procedure

Dependent Variable: force

Source	DF	Sum of Squares	Mean Square	F Value	Pr > F
Model	3	26257783.36	8752594.45	18.86	<.0001
Error	14	6497661.75	464118.70		
Corrected Total	17	32755445.11			

R-Square	Coeff Var	Root MSE	force Mean
0.801631	30.06160	681.2626	2266.222

Source	DF	Type I SS	Mean Square	F Value	Pr > F
material	3	26257783.36	8752594.45	18.86	<.0001

Source	DF	Type III SS	Mean Square	F Value	Pr > F
material	3	26257783.36	8752594.45	18.86	<.0001

The GLM Procedure

Dependent Variable: acceleration

Source	DF	Sum of Squares	Mean Square	F Value	Pr > F
Model	3	15667.31461	5222.43820	24.37	<.0001
Error	14	3000.08150	214.29154		
Corrected Total	17	18667.39611			

R-Square	Coeff Var	Root MSE	acceleration Mean
0.839288	25.29486	14.63870	57.87222

Source	DF	Type I SS	Mean Square	F Value	Pr > F
material	3	15667.31461	5222.43820	24.37	<.0001

Source	DF	Type III SS	Mean Square	F Value	Pr > F
material	3	15667.31461	5222.43820	24.37	<.0001

The GLM Procedure

Dependent Variable: time

Source	DF	Sum of Squares	Mean Square	F Value	Pr > F
Model	3	5.43794444	1.81264815	3.95	0.0311
Error	14	6.42275000	0.45876786		
Corrected Total	17	11.86069444			

R-Square	Coeff Var	Root MSE	time Mean
0.458484	27.42820	0.677324	2.469444

Source	DF	Type I SS	Mean Square	F Value	Pr > F
material	3	5.43794444	1.81264815	3.95	0.0311

Source	DF	Type III SS	Mean Square	F Value	Pr > F
material	3	5.43794444	1.81264815	3.95	0.0311

The GLM Procedure

Dunnett's t Tests for force

NOTE: This test controls the Type I experimentwise error for comparisons of all treatments against a control.

Alpha	0.05
Error Degrees of Freedom	14
Error Mean Square	464118.7
Critical Value of Dunnett's t	2.62032

Comparisons significant at the 0.05 level are indicated by ***.

material Comparison	Difference Between Means	Simultaneous 95% Confidence Limits		
ABG - Intact	251.7	-945.8	1449.2	
RCB - Intact	-1796.9	-2994.4	-599.4	***
RCA - Intact	-2677.8	-3940.0	-1415.5	***

The GLM Procedure

Dunnett's t Tests for acceleration

NOTE: This test controls the Type I experimentwise error for comparisons of all treatments against a control.

Alpha	0.05
Error Degrees of Freedom	14
Error Mean Square	214.2915
Critical Value of Dunnett's t	2.62032

Comparisons significant at the 0.05 level are indicated by ***.

material Comparison		Difference Between Means	Simultaneous 95% Confidence Limits		
ABG	- Intact	12.115	-13.616	37.846	
RCB	- Intact	-40.685	-66.416	-14.954	***
RCA	- Intact	-61.275	-88.398	-34.152	***

The GLM Procedure

Dunnett's t Tests for time

NOTE: This test controls the Type I experimentwise error for comparisons of all treatments against a control.

Alpha	0.05
Error Degrees of Freedom	14
Error Mean Square	0.458768
Critical Value of Dunnett's t	2.62032

Comparisons significant at the 0.05 level are indicated by ***.

material Comparison	Difference Between Means	Simultaneous 95% Confidence Limits	
RCA - Intact	1.1750	-0.0800	2.4300
ABG - Intact	0.4025	-0.7881	1.5931
RCB - Intact	-0.3275	-1.5181	0.8631